Gas seepage and pockmark formation from subsurface reservoirs: Insights from table-top experiments

Inbar Vaknin[1], Einat Aharonov[2], Ran Holtzman[3], and Oded Katz[4]

[1]1Institute of Earth Sciences, The Hebrew University of Jerusalem
[2]Hebrew University of Jerusalem, Israel
[3]Coventry University
[4]Geological Survey of Israel

December 1, 2023

Abstract

Pockmarks are morphological depressions commonly observed in ocean and lake floors. Pockmarks form by fluid (typically gas) seepage thorough a sealing sedimentary layer, deforming and breaching the layer. The seepage-induced sediment deformation mechanisms, and their links to the resulting pockmarks morphology, are not well understood. To bridge this gap, we conduct laboratory experiments in which gas seeps through a granular (sand) reservoir, overlaid by a (clay) seal, both submerged under water. We find that gas rises through the reservoir and accumulates at the seal base. Once sufficient gas over-pressure is achieved, gas deforms the seal, and finally escapes via either: (i) doming of the seal followed by dome breaching via fracturing; (ii) brittle faulting, delineating a plug. The gas lifts the plug and seeps through the bounding faults; or (iii) plastic deformation by bubbles ascending through the seal. The preferred mechanism is found to depend on the seal thickness and stiffness: in stiff seals, a transition from doming and fracturing to brittle faulting occurs as the thickness increases, whereas bubbles rise is preferred in the most compliant, thickest seals. Seepage can also occur by mixed modes, such as bubbles rising in faults. Repeated seepage events suspend the sediment at the surface and create pockmarks. We present a quantitative analysis that explains the tendency for the various modes of deformation observed experimentally. Finally, we connect simple theoretical arguments with field observations, highlighting similarities and differences that bound the applicability of laboratory experiments to natural pockmarks.

Gas seepage and pockmark formation from subsurface reservoirs: Insights from table-top experiments

I. Vaknin[1], E. Aharonov[1]*, R. Holtzman[2]*, O. Katz[3]

[1]Institute of Earth Sciences, The Hebrew University of Jerusalem, Jerusalem, Israel
[2]Centre for Fluid and Complex Systems, Coventry University, Coventry, United Kingdom
[3]Geological Survey of Israel, Jerusalem, Israel

Key Points:

- Sandbox experiments link pockmark morphology (irregular vs conical) to gas-seepage-induced deformation of the host (seal) layer
- Experiments and theory show seal thickness and consolidation control deformation mechanism: doming, brittle (faults), or plastic (bubbles)
- Theoretical calculations predict that under field conditions, the preferred mechanism for gas escape will be bubbles rising in faults.

Corresponding author: Einat Aharonov, Ran Holtzman, `einatah@mail.huji.ac.il`, `ran.holtzman@coventry.ac.uk`

Abstract

Pockmarks are morphological depressions commonly observed in ocean and lake floors. Pockmarks form by fluid (typically gas) seepage thorough a sealing sedimentary layer, deforming and breaching the layer. The seepage-induced sediment deformation mechanisms, and their links to the resulting pockmarks morphology, are not well understood. To bridge this gap, we conduct laboratory experiments in which gas seeps through a granular (sand) reservoir, overlaid by a (clay) seal, both submerged under water. We find that gas rises through the reservoir and accumulates at the seal base. Once sufficient gas overpressure is achieved, gas deforms the seal, and finally escapes via either: (i) doming of the seal followed by dome breaching via fracturing; (ii) brittle faulting, delineating a plug. The gas lifts the plug and seeps through the bounding faults; or (iii) plastic deformation by bubbles ascending through the seal. The preferred mechanism is found to depend on the seal thickness and stiffness: in stiff seals, a transition from doming and fracturing to brittle faulting occurs as the thickness increases, whereas bubbles rise is preferred in the most compliant, thickest seals. Seepage can also occur by mixed modes, such as bubbles rising in faults. Repeated seepage events suspend the sediment at the surface and create pockmarks. We present a quantitative analysis that explains the tendency for the various modes of deformation observed experimentally. Finally, we connect simple theoretical arguments with field observations, highlighting similarities and differences that bound the applicability of laboratory experiments to natural pockmarks.

Plain Language Summary

Pockmarks are pit-like depressions common in ocean and lake floors, formed by gas seepage through underlying sediments. Despite relevance to both fossil fuel exploration and global warming, the mechanisms by which pockmarks evolve remain elusive. We conduct simple laboratory experiments in which we inject air into a layer of glass beads ("reservoir") overlain by a layer of clay ("seal"), all submerged underwater in a transparent box. We find that gas rises through the sand and accumulates at the base of the clay. Then, gas pressure rises until it suffices to deform the clay and escape, forming a pockmark. This occurs by one of three mechanisms, depending on clay thickness and stiffness: (i) heaving of a dome which then fractures in thin clay layers; (ii) faulting in thick, stiff clays; and (iii) bubbles ascend in thick, soft clays. Pipe-like focused gas conduits connecting the clay bottom to the pockmark are created by the rise of a "trains" of bubbles that weaken their path. These pathways can also initiate in faults. Repeated seepage events push the clay particles, suspending them in water to create a pockmark. Our findings agree with field observations, improving our understanding of natural pockmark formation.

1 Introduction

Gas seepage from oceanic and lacustrine sediments is globally prevalent, forming geological structures such as pockmarks, vents, and mud volcanoes along the continental margins at many locations (Dupré et al., 2010; Schattner et al., 2012; Skarke et al., 2014; King & MacLean, 1970; Pilcher & Argent, 2007; Sultan et al., 2010; Q. Sun et al., 2012; Hovland et al., 2005; Riedel et al., 2020; de Mahiques et al., 2017; Krämer et al., 2017). Oceanic gas seeps introduce large quantities of methane into the water body, up to ∼65 Tg/yr from continental shelves alone (Skarke et al., 2014; Hovland et al., 1993). Methane venting affects ocean acidification, de-oxygenation, and thus the global climate (Archer et al., 2009; McGinnis et al., 2006; Hornbach et al., 2004; Svensen et al., 2004). In particular, methane, a highly potent greenhouse gas, has a crucial role in the global carbon cycle and has been proposed as the cause of past episodes of climate change (e.g. Dickens, n.d.; Archer et al., 2009; Westbrook et al., 2009). Many seeps originate from oil and gas reservoirs as well as methane hydrate deposits, and thus can serve to indicate their location (Abrams, 2005). These make the study of gas seeps "one of the most important fields in marine geology" (Berndt, 2005).

Gas seepage from the seafloor occurs via two main mechanisms: (i) diffuse capillary invasion through the sediment pores (especially in coarse-grained sediments); or (ii) focused preferential flow paths, along pre-existing faults and cracks or "pipes" opened by deformation induced by the fluids themselves as they migrate (Jain & Juanes, 2009; Fauria & Rempel, 2011; Holtzman et al., 2012; Z. Sun & Santamarina, 2019). The latter typically release large amounts of gas in an episodic and/or cyclic manner (Hovland et al., 2002, 2010), and are associated with pockmarks as well as vents and mud volcanoes. Pockmarks (PMs) are of particular importance due to their abundance as well as their role as markers for gas-induced sediment deformation and breaching which leads to seepage (King & MacLean, 1970; Schattner et al., 2016). Despite the importance of PMs as the surficial manifestation of the gas seepage, the mechanisms and the consequent spatiotemporal signature of the seeps remain elusive (Hovland et al., 2010). Here, we use laboratory experiments and theoretical analysis to expose the links between gas-induced sediment deformation, seepage, pockmark formation and their spatiotemporal evolution.

1.1 Field observations of pockmarks and gas pipes

Pockmarks are depressions within the surface of oceanic and lacustrine sediments, where their formation mechanism is believed to be tightly linked to the fluid seepage mechanism feeding them (King & MacLean, 1970; Schattner et al., 2016). PM diameters can range between meters and hundreds of meters. They are widespread in continental shelves (Schattner et al., 2012; Schattner et al., 2016), slopes (Bøe et al., 1998; Gay et al., 2006; Pilcher & Argent, 2007), the deep abyss (Camerlenghi et al., 1995; A. G. Judd, 2003), deep-sea fans (Bayon et al., 2009; Loncke & Mascle, 2004), lakes, bays, estuaries (García-Gil, 2003) and fjords (Hovland et al., 2002; Forwick et al., 2009). Within seismic cross-sections, PMs are often associated with feeding pipes of incoherent signature, which suggest gas presence or liquefied or disturbed sediments (e.g. Cartwright & Santamarina, 2015).

Field observations suggest that the morphology, spatial distribution, and temporal characteristics of PMs are controlled by the geological context in which they are formed (Pilcher & Argent, 2007). Their presence and morphology are tightly linked to the fluid escape mechanisms that feed them (Cartwright et al., 2007). Pockmarks can be generally categorized according to their morphology into two types (Fig. 1): (i) conical depressions termed "Type-1"; and (ii) shallower, more irregular and distorted "Type-2" pockmarks (Riboulot et al., 2016). In Type-1, the sediment in the center of the structure is completely removed or in suspension, while the pockmark walls retain an angle of repose; this suggests that the sediment underwent a more granular or plastic defor-

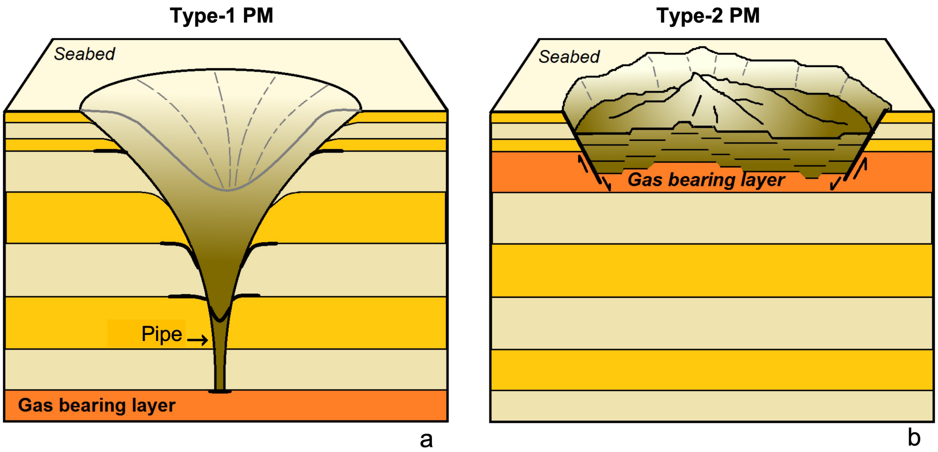

Figure 1: Geometrical characteristics of the two types of pockmarks: (a) Type-1 pockmarks are circular depression, associated with a gas pipe; (b) Type-2 pockmarks are irregular and distorted depressions.

mation (Cathles et al., 2010). In contrast, in Type-2 pockmarks both the original strata and the disrupting faults are easily recognized, suggesting a more solid-like or brittle deformation. The significant difference in the structure of the two types suggests a different formation mechanism, such as the origin of the emitted gas: Type-1 usually originates from deeper oil and gas reservoirs (Cathles et al., 2010), whereas Type-2 has been associated with near-surface gas hydrate layers (Riboulot et al., 2016). Although Type-2 pockmarks are found in many sites (Dillon et al., 1998; Sultan et al., 2010; Macelloni et al., 2012; Simonetti et al., 2013; Riboulot et al., 2016) they are far less common than Type-1.

1.2 Potential formation mechanisms of pipes and pockmarks

Several mechanisms have been proposed for the formation of fluid escape features and their associated pockmark structures (Cartwright & Santamarina, 2015):

(i) Hydraulic fracturing: this mechanism assumes fluid overpressure within or under a brittle sediment layer. If the fluid pressure rises, it may fracture the overlying seal, propagating a network of hydraulic fractures toward the surface. The accumulated and connected fractures form a breccia pipe. Growth in this case is suggested to culminate in explosive venting, leaving a dent at the surface (Moss & Cartwright, 2010; Plaza-Faverola et al., 2010, 2011; Løseth et al., 2011; Davies et al., 2012). We note that this mechanism is not supported by laboratory experiments.

(ii) Capillary barriers forming a flat piston: in this mechanism, proposed by Cathles et al. (2010), gas rises in a water-saturated reservoir and accumulates at its top, capped by an overlying low permeability seal. Since the seal is water-saturated and has a much smaller grain size than the underlying reservoir, the gas-water interface at the base of the seal forms a "capillary barrier" (Morel-Seytoux, 1993) which resists both the ascent of gas and the descent of water. As gas pressure rises it will plastically deform the seal, forming an upward-propagating capillary barrier that acts as a flat-roofed gas "piston". The invasion and upward propagation of the piston requires liquefaction of the sediment in front of it (Varas et al., 2011; Ramos et al., 2015). Cathles et al. (2010) estimated that once the piston ascends halfway to the surface its ascent accelerates, and once the piston gets close to the seafloor a PM of width similar to the piston forms rapidly.

Although in our experiments (below) we do observe the formation of pistons at the reservoir-seal interface, they do not propagate towards the surface, as predicted by Cathles et al. (2010). (Nor are we aware of any previous experiments in which a piston ascends.)

(iii) Erosive fluidization: sediment fluidization occurs when pressure gradients exerted by pore fluids on sediment grains (“seepage forces”) exceed the lithostatic stress that holds the grains in place. Seepage induced fluidization has been suggested to form PMs and mud volcanoes (Brown, 1990; Nermoen et al., 2010). Within this mechanism, one can include also the ”pore-fluid escape” mechanism that occurs during compaction-induced dewatering (Harrington, 1985; Böttner et al., 2019). Cone-shaped structures, which widen towards the surface, such as the Type-1 PMs and the associated feeding pipe in Fig. 1A, are often observed in the field (Riboulot et al., 2016). Similar cone-shaped structures have been shown experimentally to form under a high upwards fluid flux through submerged grain layers (Varas et al., 2009, 2011; Ramos et al., 2015). Such seepage-driven pipe formation may explain why pipes have a minimum distance between them, set by a lateral drainage distance from the overpressurized gas zone (Moss & Cartwright, 2010). If near-surface sediment is fluidized, grains may be ejected to the water column and deposited on the PM crater shoulders (Varas et al., 2009). Such sediment ejection in natural PMs is indicated by sonar data from the North Sea indicating massive plumes of suspended sediments above pockmarks (A. Judd & Hovland, 2009). Despite the supporting morphological field evidence, this mechanism remains controversial as it was argued that the initiation of seepage-induced fluidization requires high fluid seepage velocity (i.e. a jet) that cannot be initiated in layered sediments (Cartwright & Santamarina, 2015).

(iv) Decompaction: Two-phase systems consisting of grains and a liquid (with no gas) have shown the spontaneous formation of high permeability fluid escape pipes, forming by decompaction of the grains at the tip of upwelling bubbles (”solitons”) comprising buoyant fluids (Räss et al., 2018). When rising pipes reach the surface they form pockmarks. This process requires non-linear rheology of the sediments and has not yet been observed experimentally.

(v) Flow along existing fractures: gas utilizes existing high permeability faults and fractures to escape from depth (Hustoft et al., 2007; Berndt et al., 2003; Lawal et al., 2023). This process, comprising gas ascent in ”pockets”, followed by the collapse of fluid-filled cavities or conduits, (also evident in some of our experiments described below), was used to explain observed microseismic events below the Marmara sea (Tary et al., 2012).

(vi) Gas hydrate dissociation and volume loss: This mechanism considers a large body of gas hydrates that accumulates under, and initially inflates (forming a dome), an overlying layer of low permeability sediments. If the hydrates dissociate due to changes in temperature or pressure, the region may collapse, creating an irregular crater (Riboulot et al., 2016). This is hypothesized as the mechanism forming Type-2 PMs and based on seismic data of pockmarks from the Niger Delta where gas hydrates are abundant. We point out that free gas, even with no gas hydrate source, can also form a dome in soft sediments simply by buoyancy, as observed in offshore New Zealand (Koch et al., 2015), such that the consequent emergence of gas seeps and dome failure can produce Type-2 PMs, as will be shown in the experimental results below.

1.3 Nature of seepage through natural pockmarks

Continuous measurements of pockmark activity in the field are rare, thus the mode of activity of most PMs is uncertain. Observations suggest both continuous seepage (Hovland & Sommerville, 1985; A. Judd & Hovland, 2009) and episodic activity (Field & Jennings, 1987; Hasiotis et al., 1996; Soter, 1999; Franchi et al., 2017; Goff, 2019; Jedari-Eyvazi et al., 2023) exist at different PM locations. Linke et al. (1999) measured many orders of magnitude variability in seepage rates at the Cascadia accretionary complex. Hovland et al. (2002) suggest that most PMs exhibit dormancy as a quiescent period between activities. The source of this gas flux variability is uncertain.

1.4 Experimental and numerical simulations of pockmarks and pipes

Experiments can aid in determining which of the above multiple proposed mechanisms control the sediment breaching and associated seepage and PM formation, and under which conditions each mechanism dominates. In addition, experiments can improve understanding of the temporal and spatial evolution of PMs. Previous experimental studies of gas-related sediment breaching and PM formation mainly used a homogeneous granular medium (i.e. a single water-saturated granular layer), injecting gas at its bottom (Varas et al., 2009, 2011; Nermoen et al., 2010; Fauria & Rempel, 2011; Ramos et al., 2015; Poryles et al., 2016). For such settings, Varas et al. (2009) showed that if the injection rate is low enough, gas bubbles can ascend through the granular layer intermittently (one at a time). The zone through which the bubbles pass is fluidized, creating a cone-shaped fluidized pipe, where the wide part of the cone defines the crater near the surface (i.e., a Type 1 PM). The transition from capillary gas seepage (at high effective stress) to fracture and Type-1 PM formation (at low effective stress) has been reproduced in laboratory experiments by injecting gas into submersed unconsolidated coarse-grained sediments, and tuning the level of overpressure (and by this the level of effective stress) (Fauria & Rempel, 2011). Investigating further the influence of effective stress on deformation mode, considering the general process of gas seepage from sediments (not specifically PM formation), Z. Sun and Santamarina (2019) found that gas ascends in bubbles when the imposed confining stress is low, while it produces gas-transmitting fractures at higher confinement.

Fewer studies considered layering with a low permeability barrier. Mazzini et al. (2008) injected gas at the bottom of a 2D cell filled with porous granular media overlaid by a thin layer of clay. Gas accumulated beneath the clay until a critical overpressure was reached, leading to (i) doming at the interface between the two layers and (ii) lateral migration of the gas along the interface. Further gas injection led to dome fracturing and gas escape. Barry et al. (2012) considered similar layered settings, showing that thin-plate elasticity theory can predict the flexure and doming of the sediment layer vs. the applied gas pressure. Specifically, the authors link gas overpressure to dome geometry and material intrinsic mechanical properties (Eq. 1 in Ugural (1999).) Barry et al. (2012) found that a small deflection can already cause sediment fracture in natural domes, which may indicate why pockmarks readily form in fine-grained sediments. It was hypothesized that doming represents an early phase of pockmark formation (A. Judd & Hovland, 2009).

1.5 This study: Open questions and our approach

The above-noted studies advance the understanding of coupled gas-seepage and sediment deformation, and consequent PM formation. Yet, to date, there is no experimental exploration of the PM formation process as a whole, from its initiation, e.g. formation of gas conduits from the reservoir, to gas-induced sediment breaching, PM formation, and gas seepage. In particular, we identify the following open questions: What are the mechanical conditions for PM formation? How does PM morphology evolve with time? Is seepage through the PM episodic or continuous? How do PMs tap gas from deeply buried reservoirs? How are different PM morphologies created? What determines the size of a PM? What is the geometrical and mechanical connection between a PM and its feeding pipes?

In this paper, we present a simple experimental setup, that allows us to examine the deformation mechanisms and PM evolution under various settings. Our experimental data, which are in good agreement with theory, explain the formation process of pref-

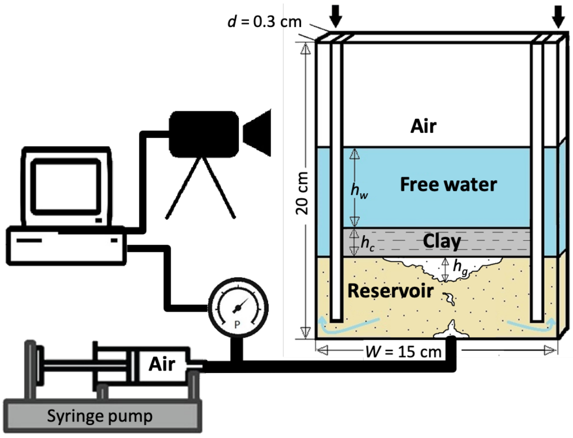

Figure 2: Schematics of the experimental setting: A quasi two-dimensional (2D) cell (thickness $d = 0.3$ cm) made of a Plexiglas transparent box, containing a thin layer of low-permeability granular media (clay) overlaying a more permeable reservoir layer (glass beads), both saturated with water. Gas (here, air) is injected using a syringe pump (where gas pressure is recorded) from a point through the lower face of the cell. Time-lapse images track the sediment deformation. Partitions at sides are used to allow free water drainage (wide arrows), ensuring that overpressure is due to the gas only (avoiding hydrofracturing). We use 2 experimental cell widths, W, 15 and 50 cm.

erential seepage pathways and the episodic, multi-stage, nature of PM generation, and shed light on how different sediment breaching mechanisms result in different types of PMs. Finally, we compare our results to field observations of pockmarks, presenting a simple theoretical analysis that exposes differences and similarities between laboratory and field settings and helps evaluate the applicability of laboratory experiments to natural pockmarks.

2 Experimental setup: Table-top pockmarks

We model submarine gas seepage using a rectangular, quasi-2D transparent Plexiglas cell (15 x 20 x 0.3 cm). filled with two water-saturated granular layers of significantly different grain size and hence permeability, acting as a reservoir overlaid by a seal (Fig. 2). All layers are submerged in water. Air is injected through a point at the center beneath the bottom layer by a syringe pump. Images of the injected gas-induced sediment deformation during the experiments are captured using a high-resolution monochrome camera at 10 Hz. The injected air pressure was measured and recorded at 1 Hz at the syringe end. Experiments ran until a stable pockmark was achieved. A clear PM structure was usually formed within 30-60 minutes, however run-time in most of the experiments did not exceed 75 minutes, a technical limitation set by the storage capacity. To test the scalability of the experiments, namely the dependence of our results on the system size, a few experiments were repeated with a larger cell (52 x 26 x 0.3 cm), recording images at 5 Hz.

The bottom ("reservoir") layer consists of tightly packed glass beads (RETSCH; diameter range 0.75-1 mm). To ensure a uniform and repeatable packing, after pouring the beads, as they start submerging, the cell was shaken vertically by hand until the beads locked and the matrix solidified. The overlaying ("seal") layer consists of natural kaolinite clay (Sigma-Aldrich) poured into the cell in suspension (fluidized in water), left to settle for either 3 or 6 weeks, to test the effect of the degree of consolidation and seal rigid-

Table 1: Summary of experimental conditions and results.

Test #[a]	Clay (cm)	Sand (cm)	Water (cm)	Settle time, t_s (weeks)	Failure mode[b]	Pockmark type	Run time (min.)
4A	0.7	5.0	5.3	3	D	2	60
3A	0.9	5.1	6.3	3	D	2	58
4B	0.9	7.0	5.2	3	P	1	52
5A	0.9	7.0	5.2	3	D+P	1	30
5B	0.9	7.0	5.2	3	D+P	1	30
3E*	1.0	5.0	5.2	3	P	1	60
2A	1.4	7.5	6.1	3	P	1	60
2B	1.4	7.1	5.6	3	D+B	2	33
3B	1.6	4.8	5.4	3	P	1	22
4C	1.6	7.0	5.2	3	P	1	57
2E*	1.6	5.0	16.9	3	P	1	43
2C	2.2	7.0	5.0	3	B+P	1	56
2D	3.8	7.0	5.2	3	P	1	43
3C	3.8	4.9	5.3	3	P	1	54
4D	5.0	5.0	5.3	3	P	1	54
4E*	10.0	6.8	5.2	3	P	1	130
1A	0.7	7.0	6.4	6	D	2	40
1B	1.2	7.1	5.9	6	D+P	2	45
5E*	1.7	5.0	16.8	6	D	2	60
1C	1.8	6.7	5.2	6	B	1	35
1E*	2.0	7.2	10.3	6	B	2	66
5C	2.2	5.4	5.5	6	B	1	73
5D	2.2	5.3	5.5	6	B	1	83
1D	2.5	5.5	6.5	6	B+P	1	60

[a] * = Wide experimental cell (W = 50 cm); in all other cases we use W = 15 cm
[b] D = Doming; B = Brittle; P = Plastic

ity. Between the sand and the clay layers, we placed a thin (∼1 mm) layer of 0.1-0.2 mm glass beads (RETSCH), to prevent downward leaching of the fine clay into the coarse reservoir layer. To ensures that the overpressure that develops in the cell is due to gas overpressure alone, as well as to avoid hydraulic fracturing of the clay by highly pressurized water trapped beneath the low-permeability clay, we install narrow partitions at both sides of the experimental cell. These side partitions allow the water to drain freely releasing water, while preventing gas flow and depressurization. This procedure ensures that the overpressure that develops in the cell is due to gas overpressure alone.

We conducted 24 individual experiments varying the thickness of clay layers (6 values; note that the sand layer thickness was also varied but this parameter is not important), clay settlement duration (2 values), and cell size (2 values). The experimental setting as well as the emerging deformation mode and pockmark type of each experiment are summarized in Table 1, where the experimental parameters and their values are listed in Section S2 (SI). The repeatability of the experiments was verified based on two sets of runs with similar initial experimental conditions. Indeed, each set resulted in similar deformation modes (4B, 5A and 5B; 5C and 5D, see Table 1). However, the specific details of the sediment deformation patterns and pressure at failure slightly differed, as expected due to unavoidable randomness in packing. We classify the PM type visually according to its geometry at the end of the experiment: (i) Type-1—regular, conical, U-shaped depressions that are empty of sediments; and (ii) Type-2—irregular depressions hosting faulted and deformed sediment.

3 Experimental results

3.1 Modes of seal breaching and gas seepage

In all experiments, we observed similar stages of gas *seepage*: (1) gas ascended through the (sand) reservoir and accumulated under the overlaying seal (clay) layer; (2) pressure progressively builds up with the continuous gas injection and accumulation, until the threshold for seal failure is met (Fig. 3); (3) the gas then seeps upwards and finally a pockmark is formed. However, the seal *failure* mode, which depends on clay layer thickness, h_c, and duration of clay settlement before injecting the gas, t_s (controlling its rigidity), differed among experiments, ranging from (i) doming, where the sealing layer bends and later breaches, allowing the escape of ascending gas through Mode I fractures; to (ii) brittle, where ascending gas pressure induced shear (Mode II) faults which served as pathways for gas escape; to (iii) plastic, where gas bubbles bouyantely rose through liquefied sediments.

Doming was the dominant mechanism in experiments where the clay was thinner and/or more rigid, and progressed according to the following stages (e.g. experiment #1A in Fig. 3 and Movies S1 and S2 in SI): (I) pressure build up in the interlayer gas pocket; (II) the overlying clay layer bends to form a dome; (III) the dome fractures by Mode I (opening) fractures and breaches; (IV) gas enters the fractures of the breached dome, widening them and seeps through; (V) The dome is deflated, causing clay blocks to collapse inward; (VI) gas continues to seep episodically through the gaps between the clay blocks, progressively disintegrating and eroding them, resulting in suspension of clay particles. Eventually, a shallow crater is created hosting collapse blocks, namely a Type-2 pockmark. In most cases, stages I–III take several minutes. Complete deflation and internal collapse of the dome (stages V–VI) require multiple gas seepage episodes. Blocks tend to interlock and can be rotated and displaced, such that a subsequent breaching of the dome and collapse requires an additional gas pressure buildup.

Brittle deformation was the dominant mechanism in experiments with intermediate thickness, rigid clay layer, and was observed to evolve in the following manner (e.g. experiment #5D, Fig. 3 and Movie S3 in SI): (I) pressure builds up to a critical point (see pressure evolution in section S1 in SI); (II) gas invades the clay layer by displacing and compressing it to create a "piston" at the base of the clay layer, in agreement with the prediction in Cathles et al. (2010). A cavity (gas bubble) starts to form within the clay, creating a mound at the top of the clay layer; (III) the gas bubble continues to grow, mostly upwards, and two sub-vertical faults appear (more noticeable at the top part of the clay), defining a free block (plug); (IV) the gas uplifts the clay block, in a piston-like motion ; (V) then, gas seeps through one of the faults, along which the clay disintegrates and liquefies; (VI) with continued seepage, the plug disintegrates entirely and a U-shaped Type-1 PM forms.

Plastic deformation of the clay was dominant in experiments in which the sealing layer was relatively thick, e.g. #2D (Fig. 3) and #4E (Fig. 4), and in which the clay had less time to solidify. Deformation generally evolved in the following manner (experiment # 2D in Fig. 3 and Movies S4 and S5 in SI): similar to the case of the brittle deformation, (I) gas invaded the clay layer by displacing it to create a 'piston' (Fig. 4), after which (II) a bubble starts to grow within the clay at the edge of the piston (Fig. 4a), forming a mound at the top of the clay layer. Then, (III) the bubble detached from the main gas reservoir at the sand-clay boundary and migrated upwards, distorting the clay (Fig. 4a); (IV) the bubble continued to migrate upwards towards the top of the clay layer, while the clay rearranges around the bubble; (V) the bubble erupted at the top of clay layer, dragging and suspending clay particles (Fig. 4b); (VI) after a series of repeated episodes of bubble eruption a significant amount of clay was removed such that a noticeable U-shaped crater i.e. Type-1 PM formed, resembling the one formed by the plug-like brittle deformation. This stream of individual bubbles progressively weakened the

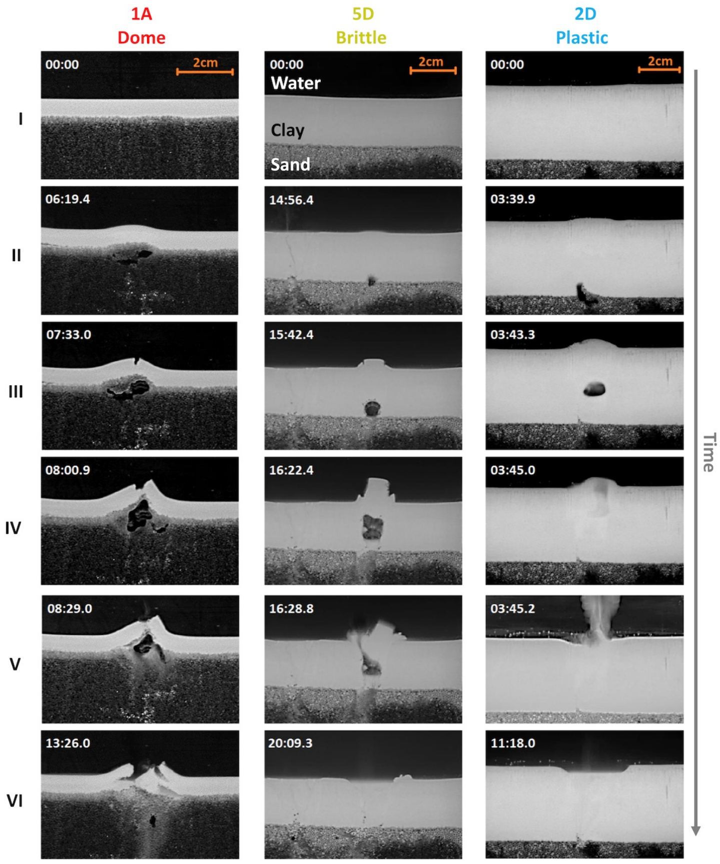

Figure 3: Snapshots showing the main stages of gas escape through a seal (gas accumulation at the seal-reservoir interface, seal breaching, gas seepage through the seal, and pockmark initiation) in three representative experiments of increasing clay layer thickness h_c (see Table 1 for details). The three experiments exemplify the three main deformation mechanism: (Left column) **Doming** (experiment #1A, h_c = 0.7 cm) is initiated by gas accumulation at the seal-reservoir interface. When the accumulated gas causes large enough dome deflection, the dome is breached by Mode-I (open) fracturing, leading to the development of a Type-2 pockmark (see also Movie S1 in supporting information (SI)); (Middle column) **Brittle** deformation (#5D, h_c = 2.2 cm). Gas accumulation at the reservoir-seal interface produces a mound in the seal, followed by Mode-II sub-vertical faulting. Seepage then occurs through these shear faults, bounding an uplifted plug, leading to the development of a Type I pockmark (see also Movie S3 in SI); (Right column) **Plastic** deformation (#2D, h_c = 3.8cm), shows gas transmitted to the surface by ascending gas bubbles, leading to the development of a Type-1 pockmark (see also Movie S4 in SI). In each snapshot (only shown is the central part of the cell) the lower part (dark gray) is the top of the sand layer, and the middle part (light gray) is the clay (seal) layer which is overlaid by water (black). Rows I–VI correspond to progressive deformation stages since injection started (I); time (min:sec) since injection shown in upper left corner.

clay to create a damage zone (pipe) within it, serving as a conduit for further bubble migration (Fig. 4C). Bubbles continuously suspend clay from the pipe such that with time the outline of the damaged pathway or pipe becomes noticeable (Fig. 4D). The migration of the bubble through the clay layer (stages II-V) occurred within ∼5-10 s, depending on the clay layer thickness (Fig. 4A–B).

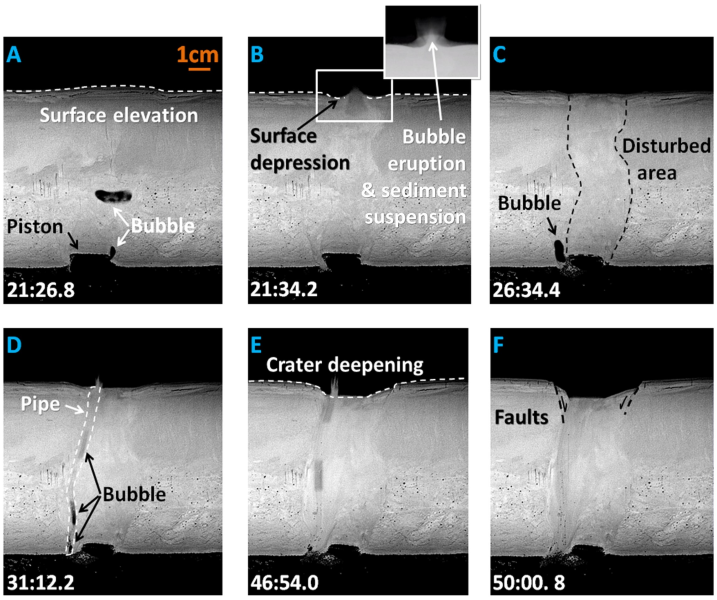

Figure 4: Experimental snapshots showing the development of a plastically-failing PM, with a feeding pipe (Experiment #4E; see Table 1 and Movie S5 in SI): (A) a piston forms with a bubble rising from its edges; (B) bubbles escape from the surface, ejecting suspended material to the water, creating a surface depression (C) bubbles initially escape from both sides of the piston, and the whole area above the piston is disturbed; (D) sequential bubble ascent creates a pipe bordering the piston; (E) episodic bubble rise through the pipe removes more material at the crater, whose borders are defined by the disturbed area; and (F) continuous development of the Type I pockmark by the collapse of the walls via faulting, interspersed by bubble escape, leading to widening of the disturbed area. The active episodes are interspersed by quiescent periods (Movie S5 in SI). Each snapshot shows the central part of the experimental cell. The lower part (black) is the top of the sand layer, and the middle part (light gray) is the clay layer which is overlaid by water (black). Time (minutes:seconds) since the start of gas flow is marked at the lower left corner of each snapshot.

We also observed mixed deformation modes: (a) doming/brittle deformation mode when a fault-bounded plug was developed in a dome (e.g. #2B); (b) doming/plastic deformation when ascending gas bubbles seep through the breached dome (e.g. #5A and 5B); and (c) brittle/plastic when an existing fault, serves as a conduit for packets of gas to escape as elongated (non-spherical) bubbles (#1D, cf. Fig. 5).

3.2 Pockmark formation and episodic seepage

Our experiments show that following the initial seal breaching, gas does not flow continuously upwards, unlike in ordinary percolation. Instead, flow pathway and pockmarks developed progressively during episodic seepage events. The intermittent nature of the deformation and seepage is also evident from the pressure temporal variations: gas pressure fluctuated in association with the evolution of the PM (cf. Section S1 in SI). We emphasize that the gas pressure measured in the inlet (syringe) is not associated with the gas pocket pressure after its detachement from the main gas reservoir and advancement into the seal layer. The evolution of PM morphology vs. number of seepage events N for each of the main deformation modes is shown in Fig. 6.

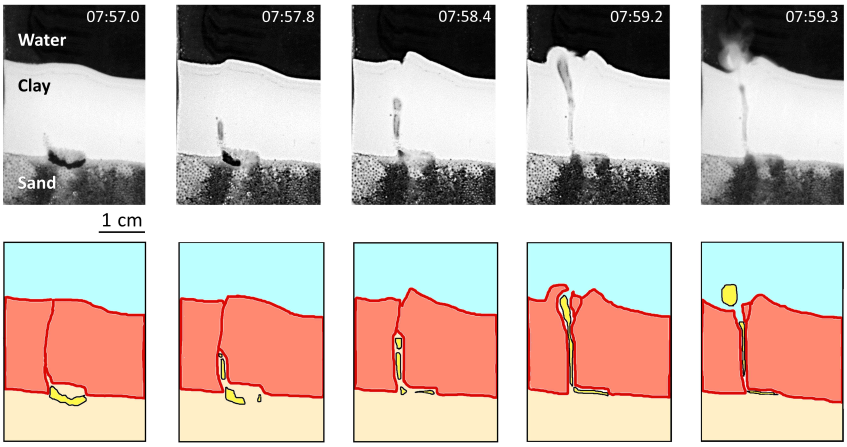

Figure 5: Experiment #1D shows a fracture and gas-filled, elongated, bubbles ascending through it. For clarity, each experimental image (top row) is accompanied by a schematic reconstructions (bottom row). The clay layer appears in white (red in the schematic), between the bottom reservoir layer in gray (yellow) and water above in black (turquoise). Bubbles appear in gray/black (yellow). Time (minutes:seconds) since the start of gas flow is marked at the upper right corner of each snapshot.

3.2.1 Type-2 pockmarks

In cases where the seal was initially deformed into a dome-shaped structure (that later collapsed), a complete Type-2 PM depression developed as a result of a sequential seepage through the debris of the collapsed dome (Fig. 6 #1A, $N = 7$–25). Type-2 PM seeps did not always occur from the same breach between adjacent blocks: gas was able to seep from different locations within the same PM, depending on the PM size and the number of blocks. Type-2 PMs either form from a wide dome that disintegrated into multiple blocks, or from small adjacent domes that merged into a single large PM (Fig. 6 #1B). As seepage continues, the blocks within Type-2 PMs were observed in some cases to gradually disintegrate, whereas in other cases PM morphology remained relatively unchanged.

3.2.2 Type-1 pockmarks

When the seal breached in a brittle or plastic manner, gas bubbles ascended through a Mode II fault or through the bulk sediment, with each seepage event deepening an erosive crater towards the development of a complete Type-1 PM. For instance, in experiments #1C and #2D in Fig. 6, the first event ($N = 1$) is seen to only slightly modify the topography, where as seepage continued clay is progressively removed from the PM zone by its suspension into the water column, making the PM shoulders clearly evident ($N = 7$; see also Fig. 4B). Further events ($N = 7$–15) make the clay below the pockmark along the seepage route looser such that it remains in suspension, until finally ($N = 25$ in Fig. 6), most of the clay is removed all the way down to the sand layer, creating a cone-shaped Type-1 PM.

In early stages, Type-1 PMs initially deepen at a relatively uniform rate, i.e. depth D increased linearly with N (Fig. 7A), irrespective of clay layer thickness h_c. The deepening rate accelerated once $D \sim 0.2$–$0.3h_c$, especially for thicker clay layers. Eventually, the PM traverses the entire clay layer, $D \approx h_c$. Occasionally, PM depth decreases (Fig.7A) due to suspended sediment or sediment from the PM rim that is falling back to the PM. The PM width L progressively increased with seepage cycles, via collapse of

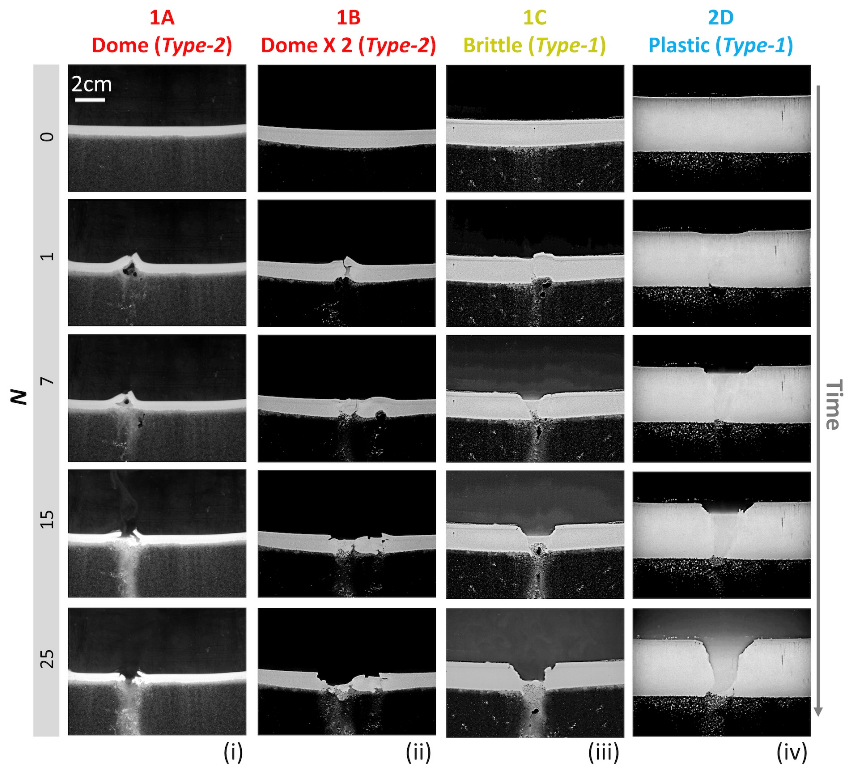

Figure 6: Experimental snapshots of pockmark development as a function of the number of seepage events, N, in four selected experiments with increasing clay thickness, h_c, exhibiting a transition in deformation mechanisms and final PM type. In each snapshot, the lower part (dark gray to black) shows the top of the sand layer, and the middle part (light gray) shows the clay (seal) layer which is overlaid by water (black). (i) Experiment #1A ($h_c = 0.7$ cm): Doming and breaching by the fracturing of the dome and development of Type-2 pockmark; (ii) #1B ($h_c = 1.2$ cm): Doming and breaching by the fracturing of a 1st dome, which is followed by the development of a second dome, its breaching and eventually development of a single Type-2 pockmark; (iii) #1C ($h_c = 1.8$ cm): Breaching by faulting, plug uplift, and development of Type-1 pockmark; (iv) #2D ($h_c = 3.8$ cm): Breaching by plastic deformation (liquefaction) around ascending gas bubble and development of Type-1 PM.

the PM walls (Fig. 7B; Movie S4 in SI). This collapse was episodic, that is not every seepage event that caused widening of the PM also resulted in collapse and deepening (Fig. 7C); collapse and deepening only occurred once the PM walls reached a critical angle. This is probably due to the hysteresis arising from the difference between static and dynamic angles of friction in granular media, i.e. in sediments (Volfson et al., 2003; Perrin et al., 2019).

In many experiments, the seepage location changed with time, creating several PMs (#1B in Fig. 6 and Movie S3 in SI). The number of seepage locations was inversely proportional to the clay thickness, irrespective of the type of seepage mechanism and domain size. When PMs were close to each other they merged to form a single wide PM. While our thin, quasi-2D experimental domain promotes PM merging by limiting the seepage location to a narrow line (vs. a surface in 3D domains), field observations of PM

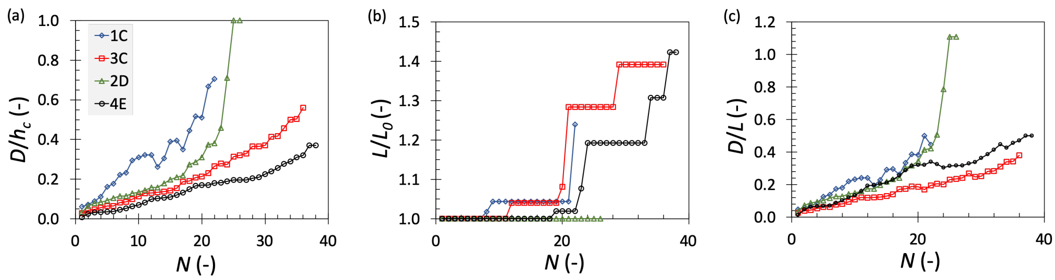

Figure 7: Quantitative analysis of the evolution of pockmark geometry vs. the number of seepage events, N, for experiments showing different deformation modes: brittle in #1C and plastic in #3C, #2D, #4E. (a) Pockmark depth, D, normalized by the clay layer thickness, h_c; (b) Pockmark width, L, normalized by its initial value, $L_0 = L(N = 1)$; (c) Pockmark aspect ratio D/L.

merger (Schattner et al., 2016) suggests that this is a viable mechanism also in more complex, 3D domains.

3.3 Experimental phase diagram of pockmark formation

The experimentally-observed deformation mechanisms and resulting structures as a function of the clay layer properties—clay thickness, h_c, and settling time, t_s, is presented as a phase diagram in Fig. 8 (see details of the experimental settings in Table 1). This diagram demonstrates the dependence of the deformation mode on the clay properties: (i) **Domes** occurred only in very thin layers ($h_c < 1$ cm) in the narrower experimental boxes ($W = 15$ cm; used for most experiments), and at a wider range of clay thickness ($h_c < 2$ cm) in the wider cells ($W = 50$ cm); (ii) **Brittle deformation** was dominant in thicker and stiffer layers (that settled longer, $t_s = 6$ weeks); and (iii) **Plastic deformation** (by bubble migration) was observed in thicker, softer ($t_s = 3$ weeks) clays.

4 Theoretical prediction of deformation mechanisms

This section provides a predictive quantitative analysis of the mechanisms for seal deformation and breaching observed experimentally: doming, brittle, and plastic deformation. The parameters and the values used for the calculations are provided in Section S3 in the SI. In our experiments, the gas injected into the bottom of the coarse grained (reservoir) layer, rises through it and accumulates under the overlaying clay. Due to the large capillary pressure required to invade the small pores in the clay, gas remains trapped as a gas pocket, also serving as a “capillary barrier” which blocks the upwards flow of water (Morel-Seytoux, 1993). The gas overpressure driving the deformation, $\Delta P(z) = P_g(z) - P_w(z)$, is defined as the difference between the pressure of the gas pocket and of the water at height z, $P_g(z)$ and $P_w(z)$, respectively. In computing it, we assume hydrostatic pressure distribution in the water column, as the side valves in our setup enable rapid release of water pressure to maintain hydrostatic conditions (Fig. 2). We stress that, even in a fully hydrostatically balanced system, buoyancy forces can create overpressure (Osborne & Swarbrick, 1997). To illustrate this, consider a gas pocket of height h_g disconnected from the syringe (Fig. 2). At the base of the gas pocket, the gas pressure is equal to that in water-saturated (gas-free) regions at a similar depth. Inside the gas pocket, the pressure decreases with elevation as $-\rho_g g h_g$, i.e. more gradually than in the water phase (P_w decreases as $-\rho_w g h_g$), where ρ_w and ρ_g are the density of water and gas respectively, and g is the gravitational acceleration. This implies that the gas overpressure at the bottom of the clay is proportional to the height of the gas pocket,

$\Delta P = (\rho_w - \rho_g) g h_g$. As the volume of the trapped gas pocket increases and h_g grows, ΔP at the top of the pocket increases until it suffices to deform the seal. It is possible that in our experiments there was a connected gas pathway from the syringe to the base of the seal; this could not be deduced from image analysis. In such a case, gas overpressure would exceed that arising from buoyancy (hydrostatic) forces alone.

The stress in the clay is computed assuming lithostatic distribution, i.e. that the clay grains support their own weight plus the weight of the water, $\sigma_{v,\text{lit}} = \rho_c h_c g + \rho_w h_w g$, where ρ_c is the saturated clay density, h_c is the clay thickness, and h_w is the water depth from the surface to the top of the clay layer (Fig. 2). Thus, the effective stress at the bot-

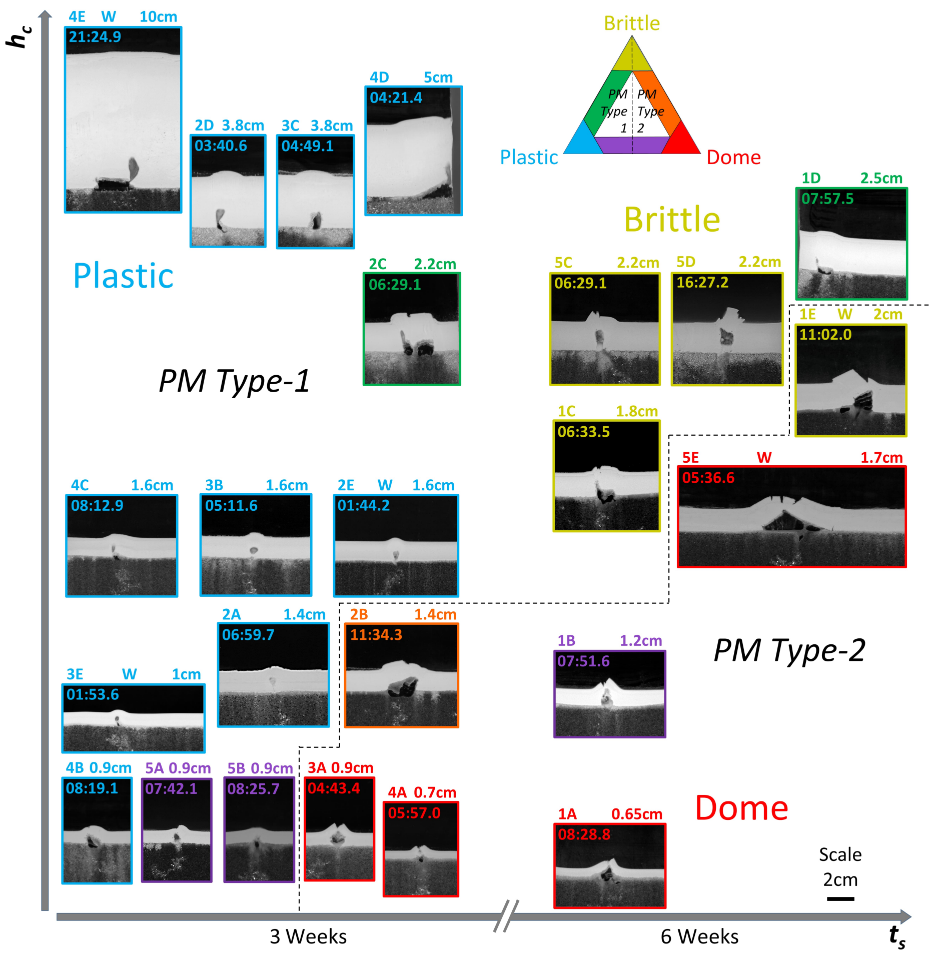

Figure 8: Experimental phase diagram of deformation mechanisms vs. settings in terms of clay thickness, h_c, and settling time, t_s. Final pockmark geometry is shown for 14 experiments, including (top row) the experiment number (left), “W” if the wider (50 cm) cell was used, h_c (right), and the time elapsed since seepage initiation (hh:min), below. The diagram is divided into PM Type-2 domain and Type-1 domain, where the boundary is marked by a dashed line. The axes are not up to scale, i.e. snapshot locations are relative: higher indicates larger h_c, and left and right correspond to t_s is 3 or 6 weeks, respectively. Snapshots are color-coded by formation mechanism (see the phase triangle): doming (in red); brittle plug development and seepage through fractures (yellow); plastic deformation by bubbles (blue); mixed doming/plastic mode (purple); mixed doming/brittle (orange); mixed brittle/plastic (green).

tom of the saturated clay layer is

$$\sigma'_v = (\rho_c - \rho_w)h_c g. \quad (1)$$

Clay deformation in our experiments occurs much faster relative to the flow and pressure relaxation of water in the clay, such that we consider undrained conditions (in contrast to the assumption in Cathles et al. (2010)). This can be justified by scaling: we observe clay deformation within seconds—the time for a bubble to traverse the clay layer by deforming it (e.g. see fig. 3, right column). The timescale for the flow across the layer can be evaluated from Darcy's law. We note that clay permeability can span a large range, 10^{-20}–10^{-14} m^2, (Chapuis & Aubertin, 2003; Neuzil, 1994); using the higher value of 10^{-14} m^2 provides the lower bound for the flow timescale. The gas pressure difference between the bottom and the top of the clay was not measured; we use instead the upper bound for gas pressure in the experiments, ∼2 kPa (Fig. S1 in SI). Assuming porosity of 0.1 and $h_c = 10$ cm, provides an upper limit of ∼1 μm/s for the velocity of water drainage from the clay, corresponding to ∼10^5 s (across a distance of $h_c = 10$ cm),4 orders of magnitude longer than the time of deformation. This justifies our undrained assumption.

In the Sections below, we derive theoretical expressions for the conditions required for each mode of clay deformation, relying on the "critical state soil mechanics" theory (Wood, 1991). Details and parameter values are provided in Section S2 in the SI.

4.1 Dome breached by fracturing

Consider an elastic dome, breached by a fracture when deflection becomes large enough (as in experiments # 1A, 5E, 4A, 3A in Fig. 8). The conditions for this mechanism are evaluated using analytical expressions from the three-point beam flexure theory (Bower,

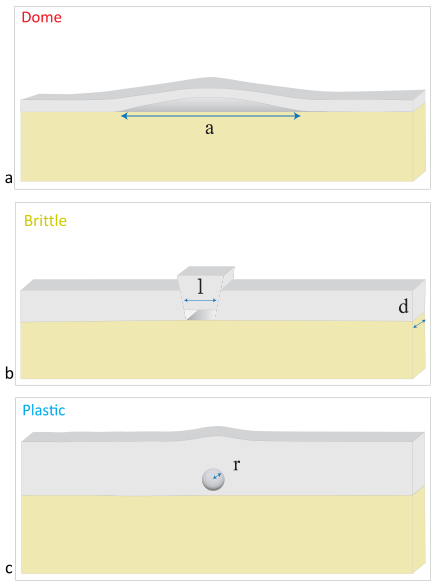

Figure 9: Characteristic length scales used in the analysis of the different seal breaching and deformation modes: (a) gas pocket forming a dome (dome width: a); (b) faults creating a plug (of base length l and thickness d), lifted by a gas pocket; (c) gas bubble (of radius r) rising within the clay.

2009). This theory computes the deformation of a rectangular beam loaded at its middle while supported at its edges. Beam failure occurs when the strain at its outer (curved) edge exceeds its tensional strength. This scenario is used as an approximation for our quasi-2D experiments, where the gas pushes the clay seal from below approximately at its centre (experiment #1A in Fig. 3, and # 1E, 5E in Fig. 8). The pressure required to fracture in tension a beam (dome) of length a (Fig. 9a) by a pressure ΔP_{dome} is (Bower, 2009)

$$\Delta P_{\text{dome}} = \frac{2}{3}\frac{{h_c}^2(\sigma_v' + T_0)}{Wa} \tag{2}$$

where T_0 is the clay tensional strength and W is the cell width.

4.2 Brittle deformation

Brittle failure occurs in our experiments via formation of a a block bordered by faults (”plug”), e.g. see experiment # 5D in Fig. 3 and #1E, 1C, 5C in Fig. 8. The first step in creating a plug is by forming a gas “piston” (see elaborated discussion in Section 4.3.1). In brittle layers, upward piston motion produces sub-vertical side faults that delineate the plug. The plug is then lifted by frictional sliding along the faults (#1A, 1C, 5C in Fig. 8). The fractures surrounding the plug—which is often tilted—act as gas escape pathways.

The gas overpressure required to induce faulting that creates and lifts a plug, ΔP_{plug}, must overcome two forces: one to create faulting in the clay layer, F_{frac}, and another to slide the plug upwards on the 2 faults delineating it, F_{slid}.

$$\Delta P_{\text{plug}} = \max\left(F_{\text{frac}}, F_{\text{slid}}\right)/A_b. \tag{3}$$

Here $A_b = dl$ is the area of the plug base, d is the spacing between the plexigalss walls, and l is plug length (Fig 9B). The shear force required to create a fault is related to the gas pressure via $F_{\text{frac}} = A_b \Delta P_{\text{frac}}$, which in turn can be obtained from the criterion for fracturing of clay by shear (Marchi et al., 2014),

$$\Delta P_{\text{frac}} = \sigma_3' + nc_u = \sigma_v' + nc_u. \tag{4}$$

Here n is an empirical coefficient of order unity (Atkinson et al., 1994). In Eq. (4) and the calculations hereafter, we assume $\sigma_3' \approx \sigma_v'$. The undrained shear strength of clay is (Eq. 8 in Mayne (2001))

$$c_u = 0.5\sigma_v' \sin(\phi)(OCR)^\gamma, \tag{5}$$

where ϕ is the undrained friction angle, OCR is the overconsolidation ratio, and σ_v' is the effective stress, given by Eq. 1 for clay seal base. The exponent γ is found empirically (Z. Sun & Santamarina, 2019). For the selection of parameter values, including ϕ, n, γ and OCR, see section S2 and Table 2 in SI.

The sliding force F_{slid} in Eq. 3 is computed as the sum of the following forces: (i) frictional resistance to the sliding of the plug against its two bordering faults (assumed to be sub-vertical), $2\sigma_v'\mu_c h_c d$; (ii) frictional resistance with the cell walls, $2\sigma_v'\mu_w h_c l$; and (iii) the force to lift the plug weight, $\sigma_v' A_b$:

$$F_{\text{slid}} = \sigma_v'(2\mu_w h_c l + 2\mu_c h_c d + dl) \tag{6}$$

where μ_c and μ_w are the clay-clay and clay-wall friction coefficients, respectively (see Section S2 in the SI). Substituting F_{frac} and F_{slid} into Eq. 3 provides the critical pressure for brittle deformation,

$$\Delta P_{\text{plug}} = \max\left[\sigma_v' + nc_u, \sigma_v'(2\mu_w\frac{h_c}{d} + 2\mu_c\frac{h_c}{l} + 1)\right]. \tag{7}$$

4.3 Plastic deformation

The third possible mode of seal failure is the creation of a cavity by plastic deformation (9C). This cavity may form by the rise of either a "piston" or a gas bubble (Fig. 4A). In thin clays (#4C, 2E, 3B in Fig. 8) bubbles are created at the bottom or middle of the clay layer. In thicker clays bubbles are often generated from tips of a flat piston (Cathles et al., 2010) that first yields into the clay (Fig. 4; Fig 8 #4C, 4D). The conditions for the different stages of plastic deformation are computed below.

4.3.1 Piston formation

In some of the experiments with thick seals, a "piston" developed above the large gas pocket pushing into the clay seal. The piston, shaped by the capillary forces associated with interfacial tension, has a relatively flat top and limited width. Cathles et al. (2010) hypothesized (i) the development of such a piston; (ii) that the piston dimensions depend on the pore size distribution; and (iii) the rising piston will liquefy the sediments above it, allowing it to accelerate upwards. Our experiments indeed demonstrate that in some cases a piston is created, and our calculations below predict that it will liquefy the clay above it. However, we do not observe an acceleration of the piston; instead, we observe that the piston comes to a halt, and the trapped gas escapes via bubbles emanating from its edges (Fig. 4). Bubble formation at the edges is aided by stress concentration at the sharp edges of the piston. The conditions for this mechanism are quantified below.

4.3.2 Bubble and cavity formation

The pressure required to form a gas-filled cavity (bubble or piston) in the clay is

$$\Delta P_{\text{cavity}} = \sigma'_v + 1.3c_u \left[1 + \ln\left(\frac{E}{2c_u(1+\nu)}\right)\right], \tag{8}$$

where E and ν are Young's modulus and Poisson ratio of the clay (Z. Sun & Santamarina, 2019). Eq. 8 implies that ΔP_{cavity} always exceeds the liquefaction threshold, $\sigma'_v + c_u$, supporting the hypothesis that clay will be liquefied around the cavity. Liquefaction allowing bubbles to ascend by pushing the clay in front of them was observed experimentally by Varas et al. (2011); Ramos et al. (2015). Furthermore, as both ${\sigma'}_v$ and c_u are proportional to clay thickness h_c (Eqs. 1, 5), Eq. 8 suggests a that the pressure of the bubble or piston also increases with h_c, as confirmed by our experimental data (Fig. S2 in the SI).

4.3.3 Bubble ascent

A gas bubble will continuously grow in place until the buoyancy force overcomes the drag force, allowing it to ascend (Fig. 10). Bubble ascent requires an additional force (beyond that required for bubble formation and liquefaction) to overcome the drag force resisting the bubble motion within the clay. The drag force is estimated here via dimensional analysis,

$$F_d = kc_u\pi r^2, \tag{9}$$

where r is bubble radius and k is an empirical parameter. The buoyancy force acting to lift the bubble is computed from the weight of the submerged clay it displaced, of volume similar to that of the bubble, $4/3\pi r^3$:

$$F_b = (\rho_c - \rho_w)\frac{4}{3}\pi r^3. \tag{10}$$

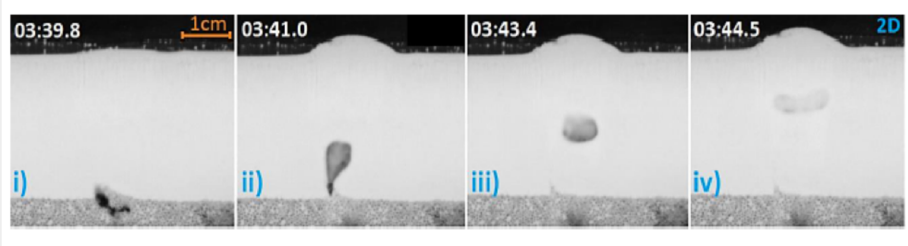

Figure 10: Four stages of bubble migration in clay (experiment #2D): (i) Gas invasion, (ii) bubble vertical growth and detachment, (iii) rounded bubble migration, (iv) bubble flattening due to its movement upwards. In each snapshot, the lower part (dark gray) shows the top of the sand layer, and the middle part (light gray) shows the clay (seal) layer which is overlaid by water (black). The time elapsed since seepage initiation (hh:mm) appears in the upper left corner.

Once the bubble reaches a critical radius, $F_b = F_d$, and it starts to rise. The critical bubble radius to overcome the drag is computed from the above together with Eq. 5,

$$r_c = \frac{3kc_u}{4(\rho_c - \rho_w)} = 0.13kgh_c(OCR)^{\gamma}. \tag{11}$$

Eq. 11 predicts a dependence between the critical bubble size and layer thickness h_c, in agreement with our experimental observations (Fig. S2 in SI). We note that Eq. 11 relies on the assumption of a spherical bubble, whereas in many cases bubbles were distorted during ascent, e.g. see Figs. 5 and 10. This, together with the limited number of experimental data points, prevented a reliable estimate of k from our data.

4.3.4 Pipe and pockmark formation by bubble ascent

Bubbles ascend while liquefying the sediment in front of them. This leaves a record of the gas passage in the form of a liquefied pathway within the clay (Fig. 4), providing an easier pathway for subsequent bubble ascent (by reducing both ϕ and OCR, and hence c_u, cf. Eq. 5). Repeated occurrence of this mechanism creates a localized gas pipe (Fig. 4D, E), of a width that is correlated with the bubble dimensions. Each escaping bubble also deepens the crater (Fig. 4E and Fig 7a). As the crater walls repeatedly collapse by faulting and sliding (Fig. 7b), it forms a pockmark (Fig. 4F) of increasingly larger depth to width ratio (Fig. 7c). In some cases when fractures form, they serve as pipes for venting elongated bubbles (that fit the fracture width, cf. #1D in Fig. 5), a mixed brittle/plastic deformation mode (e.g. #2C in Fig. 8).

4.4 Transition between failure mechanisms

Following a gas pocket buildup at the base of the clay seal, gas escapes in our experiments by either (i) fracturing an elastic dome; (ii) brittle deformation, as a plug delineated by faulting; or (iii) plastically, by ascending bubbles. The dominant failure mechanism is the one requiring the least gas overpressure (e.g. Z. Sun & Santamarina, 2019), which we compute from Eqs. 2, 7 and 8. This dominant overpressure and the corresponding mechanism is shown in Fig. 11(a–b) for two clay consolidation states, $OCR = 0.5$ (a; representing short settling time of $t_s = 3$ weeks) and $OCR = 1$ (b; $t_s = 6$ weeks). These low OCR values are representative of the loose state of our system, which compacted under its own weight only. As expected, the failure pressure mostly increases with increasing clay thickness h_c. For loosely compacted clays (Fig. 11a), the mode of preferred failure transitions from dome to bubble at $h_c \simeq 1$ cm. For stiffer, more consolidated layers (Fig. 11b), the mode of failure transitions from doming to brittle faulting at $h_c \simeq 0.7cm$, and from faulting to bubbles (plastic) at $h_c \simeq 2cm$.

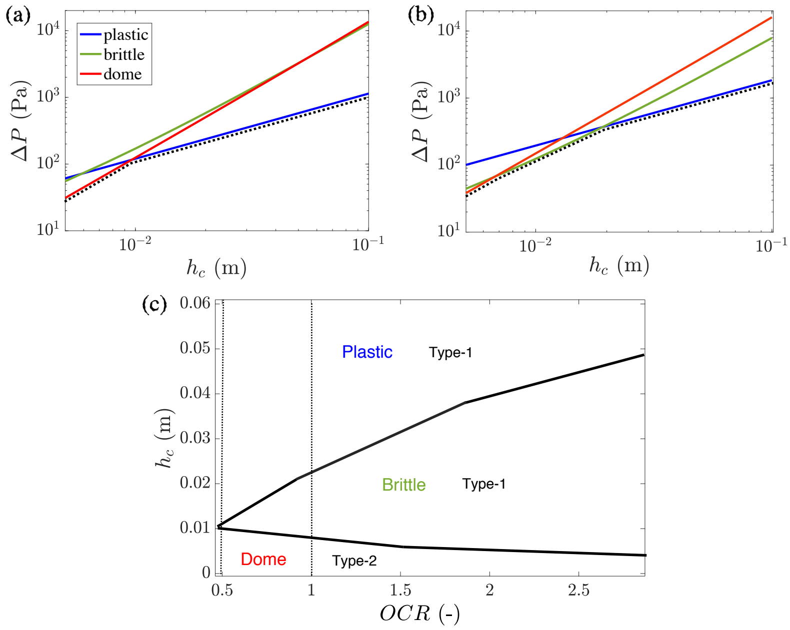

Figure 11: Calculated gas overpressure required to activate each of the 3 failure modes of the seal in our experiments (solid lines; Eq. 2 in red, Eq. 7 in green, and Eq. 8 in blue), and expected PM types, as function of clay layer thickness h_c, for two different representative consolidation degrees: (a) OCR=0.5; and (b) OCR=1. The dominant deformation mode is set by the mechanism requiring the minimal value of ΔP (dotted black lines). (c) Theoretical phase diagram for the preferred (minimal ΔP) deformation mode, as function of clay layer thickness and OCR value, adding more OCR values in addition to those shown in (a) and (b).

A phase diagram showing the expected mode of failure as a function of OCR and clay thickness h_c is presented in Fig. 11c. Values of $OCR > 1$ are of practical interest as in nature there are larger stresses that produce greater consolidation. Fig. 11c shows that domes are predicted to be the preferred deformation mode for very thin layers (here $h_c < 1$ cm). For thicker layers, the mode of failure transitions with increasing h_c, first to brittle faulting creating a plug, and then to plastic: for soft clay ($OCR = 0.5$), layers thicker than 1 cm will degas by bubbles. In more rigid clays ($OCR = 1$) layers of intermediate thickness (here $1 \le h_c \le 2.25$ cm) will degas by lifting a faulted plug, while clays with $h_c > 2.25$ cm will still degas by bubbles. As the clay compacts more (larger OCR), the transition from brittle to plastic occurs at increasingly larger h_c.

5 Discussion

5.1 Theory of seal deformation applied to experimental results

Our experiments show that the mode of deformation controls the eventual PM type: Domes lead to Type-2 PM while brittle and plastic deformation create a Type-1 PM; e.g. see Fig. 6 and 8. Our analysis (Fig. 11c) suggests that the mode of deformation and thus the eventual PM type co-depend on two experimental parameters: clay thickness h_c and settling time t_s. The time t_s controls the degree of consolidation (as measured by the OCR), thus affecting the clay elastic modulus (Eq. S2 in SI) and shear strength c_u (Eq. 5). t_s also affects the tensile strength, T_0 (Eq 2). Seal thickness h_c also affects all modes of failure, appearing directly or indirectly in all failure conditions (Eqs. 2, 3 and 8). In this way both h_c and t_s affect the strength for dome breach, and brittle and plastic failure. The theoretical phase diagram (Fig 11c) is in general in good agreement with the experimental data (phase diagram in Fig. 8). Both the experiments and the theory suggest that doming would dominate for the thinnest layers, plastic deformation by bubble ascent for the thickest layers, and brittle faulting more dominant for intermediate layer thickness, with faulting in stiffer, more settled layers. A corresponding transition from Type-2 to Type-1 PM is seen experimentally and predicted theoretically. The experiments also support the theoretical prediction that the critical clay thickness (h_c) value at the transition between Type-2 to Type-1 PM increases with the system size (width of the experimental cell); e.g. in Fig 8 experiment #5E (wider cell) is deformed by doming whereas #1C (narrower cell, nearly identical h_c) produces faulting.

Despite the overall agreement between our experimental data and theory, the theoretical critical pressure in Fig. 11(a–b) cannot be directly validated by our experiments. This is because once the gas pocket detaches from the inlet (syringe) and ascends (see e.g. Movie S1 in SI), its pressure is no longer associated with that of the reservoir (inlet, where we measure the pressure, cf. Fig. S1 in SI). Instead, we could estimate bounds: the inlet pressure provides an upper bound, whereas $(\rho_w - \rho_g)gh_g$ provides a lower bound , where h_g is the height of the detached gas pocket. The theoretical values in Fig. 11(a–b), ~100-1000 MPa, are well within the bounds evaluated from our experiments.

5.2 Theory of seal deformation applied to field conditions

The application of the theoretically predicted deformation mechanisms to field conditions and scales requires (i) extending the calculations from 2D to 3D; (ii) considering thicker seal layers, i.e. h_c of 1–1000 m (Koch et al., 2015; Moss & Cartwright, 2010); and (iii) higher stresses. The expressions predicting the critical overpressure corresponding to each deformation mode are provided below, and plotted vs. clay thickness h_c in Fig. 12.

Doming in 3D corresponds to an overpressure of (Barry et al., 2012; Koch et al., 2015),

$$\Delta P_{dome3D} = \frac{8}{3}\frac{E}{1-\nu}\frac{h_c w_{max}}{a^4}\left(\frac{2{h_c}^2}{1+\nu} + {w_{\max}}^2\right) + \sigma_v' \tag{12}$$

where $w_{\max}$ is the dome maximum vertical deflection, and a is its lateral dimension. To compute the pressure in Eq. 12 we use the parameter values for a/h_c, $w_{\max}/a$ and E from (Koch et al., 2015), as discussed in Section S3 in the SI. We note that this computation is poorly constrained by field observations due to the large uncertainty (wide bounds) in the values of the governing parameters a, $w_{\max}$ (Barry et al., 2012) and E (Koch et al., 2015). In addition, doming does not imply the mode of seal breaching, and therefore the above does not provide a critical overpressure for seepage.

Brittle deformation due to overpressure in field settings will either involve opening (Mode I failure) of pre-existing faults or fractures, or the creation of new faults (hydrofractures), through which gas will seep. "Plug-lifting" along faults, observed in some of our experiments, is not expected to occur in the field, as it is due to the small dimension of our experimental cell and our 2D settings. To lift a plug requires that the force exerted by the gas overpressure, exceeds the weight of the plug plus friction force on all four surfaces bounding the plug. Yet, these forces (stress times area) increase with system scale. Transmitting gas via an opening-mode pulse (i.e., rising penny-shaped bubbles (Boudreau et al., 2005)) only require stress to locally exceed a threshold. Thus, gas transmission through field-scale faults is expected to occur in rising disk-like bubbles, as observed in the gas-injection-into-gelatin experiments of (Boudreau et al., 2005; Boudreau, 2012), and also in some of our thick-seal experiments, e.g. Fig. 5. To open a pre-exiting fracture the gas overpressure must exceed the effective confining stress, whereas to form and open a new hydrofracture requires an even higher overpressure (cf. Eq. 4), see Fig. 12.

A bubble can rise buoyantly in fractures once its buoyancy force exceeds the drag force, where the critical bubble size depends on its shape and size, and on layer thickness (Section 4.3.3). Extending our computations relying on the assumption of a spherical bubble (Eq. 11) is beyond the scope of this paper.

Note that once one gas bubble ascends through a fault or fracture it decompacts the sediment in its pathway, locally reducing its strength (Eq. 5), which in turn favors future gas ascent within this route, localizing it into a gas pipe.

Plastic deformation by bubbles forming in intact sediment (without fracturing) in the field is expected to require the same overpressure as in the experiments (Eq. 8), see Fig. 12 (blue line).

Capillary invasion was not discussed in relation to our experiments, due to the prohibitively high capillary entry pressures in the fine clay we used as seal. The gas overpressure required to push it into water-filled pore throats of size r is

$$\Delta P_{\mathrm{cap}} = \frac{2\gamma_{gw}}{r} \tag{13}$$

where γ_{gw} is gas-water surface tension (0.072 N/m). The pore sizes in natural clays span a wide range which is hard to constrain. Fig. 12 shows an estimate for intact shale, assuming for simplicity a constant r with depth. As a rough estimate, we use the dominant pore size $r \sim 0.03\mu m$ measured in unconfined shale (Makhnenko et al., 2017), providing an overpressure of $\Delta P_{\mathrm{cap}} \sim 4.8$ MPa (horizontal dashed line in Fig 12). If r decreases with confinement (depth) ΔP_{cap} will grow.

The mode of sediment failure which will be preferred is the one requiring the least pressure. Our theoretical analysis (Fig. 12) suggests that doming will constitute the initial stage of many PMs; this agrees with the common interpretation of field-observed domes (A. Judd & Hovland, 2009; Barry et al., 2012; Koch et al., 2015). However, doming as early stage deformation model does not in itself imply the dominant mode during further seal breaching and gas seepage. Following initial doming, our theoretical analysis (Fig. 12) predicts gas escape by opening pre-existing faults and fractures (as seen experimentally, cf. Fig 5). Without pre-existing faults, hydro-fracturing is expected to occur, at slightly higher over-pressure. In domes, the overpressure required to fracture/fault the dome will be lowered relative to those required to fracture a flat seal, due to the extensional fiber stresses exerted by the dome flexure (for calculation of these stresses see Turcotte and Schubert (2014), section 3.12), but we do not further pursue this calculation due to the very variable elastic modulus value.

Following conduit opening, gas bubbles will rise once reaching a critical radius, set by layer thickness and bubble geometry, leaving an elongated weakened pipe-like structure behind. We do not expect bubbles to rise freely in *undisturbed* sediment, due to the large pressure required, which is much higher than that to create a hydrofracture.

Once bubbles, rising in faults or fractures, reach the seal surface, they may create a PM via "erosive fluidization" (Cartwright & Santamarina, 2015): gas eruption ejects sediments to the shoulder of a PM, eroding the surface and creating a depression (e.g. Figs 5 and 4). This PM formation process constitutes a combination of several different mechanisms for gas transport to the surface which were discussed earlier. We emphasize that our experiments indicate that fluidization and associated erosion do not require a fluid jet (as suggested by Cartwright and Santamarina (2015)).

5.3 Implications from tabletop experiments and theory to natural pockmarks

Our experiments uniquely observe the entire process of gas seepage from the reservoir to the surface (sea floor), i.e. the initial pressure-induced seal failure followed by the passage of gas through the seal, and finally the formation of PMs at the surface, where gas seeps out (Fig. 6). The deformation mechanisms forming the PMs differ between experimental and field conditions: In experiments either brittle failure or ascent of relatively spherical bubbles in liquefied clay can occur (depending on experimental setting), whereas in the field brittle deformation is expected to dominate, with elongated bubbles rising through fractures or faults. The observations in the field regarding the role of faulting are equivocal: while some (e.g. Crutchley et al. (2021)) suggest that gas preferentially rises through vertical fractures instead of through pre-existing faults, others show that pre-exiting faults control gas escape (Hustoft et al., 2009). The mechanisms of seal breaching and bubble ascent (Fig. 3) control not only the manner by which the gas seeps out to the surface but also the sediment suspension in the water column, the episodic nature of the seepage, and the eventual PM shape (Fig. 6). Below we compare our findings to field observations.

5.3.1 Gas migration through the sediment

Based on analysis of fluid escape pipes morphology and their geological context using seismic sections, Løseth et al. (2011) and Cartwright and Santamarina (2015) concluded that pipes play a critical role in providing leakage pathways for trapped hydrocarbons through overlying seals. Løseth et al. (2011) suggested hydro-fracturing of the seal as the main mechanism for breaching and pipe formation. In contrast, Cartwright

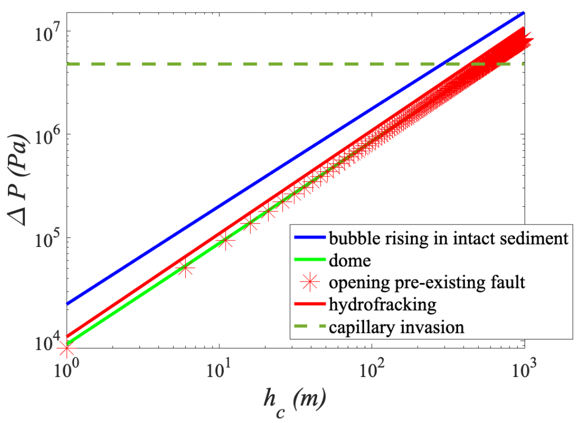

Figure 12: Calculated overpressure required to initiate deformation under field conditions. Doming (solid green line; Eq. 12) and opening of existing faults and fractures (red stars; $\Delta P = \sigma'_v$) require nearly the same overpressure, and are the 2 favored deformation modes. Hydrofracking, i.e. opening new fractures, requires only slightly higher overpressure (solid red line; Eq. 4). Gas Bubbles rising freely in the sediment (blue line; Eq. 8) are unlikely since they require much higher pressure than the brittle modes. Ignoring compaction, capillary invasion pressure is constant with depth (horizontal dashed line; Eq. 13). This phase diagram predicts that (until at least 1km depth) gas overpressure will create domes and escape by bubbles opening pre-existing fractures, if such exist. Otherwise, domes will form, followed by hydrofracking and gas ascent in bubbles through them.

and Santamarina (2015) excluded over-pressurized fluid related processes (such as hydraulic fracturing, erosional fluidization and capillary invasions) as the dominant mechanism forming pipes; instead, Cartwright and Santamarina (2015) suggested localized collapse due to volume loss and syn-sedimentary flow localization as possible mechanisms for pipe growth, where initiation might be controlled by the above over-pressurized fluid related mechanism. Our experiments support a combination of the processes suggested by Cartwright and Santamarina (2015) and Løseth et al. (2011). In our experiments we observe that during the initial stage escape features (bubbles, faults, domes) form by high pore pressure. After the initial weakened zone forms, pipes develop as disrupted zones by repeated material degradation (Figs. 3, 4). Pipes direct gas seepage from the reservoir, through the seal to the seafloor (Fig. 4), in agreement with field data in Løseth et al. (2011) showing pipes traversing throughout the seal all the way to the seafloor. Our experimental observations also agree with the model suggested by Løseth et al. (2011): overpressure buildup and release via pipes, and the formation of a mound at the pipe upper terminus, resulting in ejection of fluidized sediment close to the surface (rather than from depth). Our experiments also agree with the common hypothesis (Cartwright and Santamarina (2015) and elsewhere) relating the termination of pipes at the seafloor to PMs.

Another finding in our experiments that is relevant to field conditions is our observation of a mixed seepage mechanism, in which bubble pulses rise along brittle fractures (Fig. 5). Like the vertical gas pipes, the fractures or faults become liquefied pipes after bubbles traverse them, promoting transport of further bubble trains in these pipes. Our theoretical analysis indicates that this gas-escape mode would be ubiquitous in nature, in agreement with Z. Sun and Santamarina (2019). This theoretical prediction is supported by field data in the form of seismic micro-events in soft sediments, attributed to bubble rise and escape via faults (Tary et al., 2012).

In terms of bubble geometry, our experiments show that the rising bubbles are flattened into disk shapes (Fig. 5), similar to the reports in natural sediments by Marcon et al. (2021), and to the Boudreau et al. (2005) experiments of gas injection into gelatin. Furthermore, bubble disk radii were seen in our experiments to correlate with pipe widths, as seen in Figs. 4D and 5 (Note that the final localized pipe width may be much narrower than the initially disturbed zone width, as shown in Fig 4D). Thus, pipe widths are expected to grow with bubble radii, which in turn increase with seal layer thickness (experimental observation showing increasing of bubble radius with clay thickness are presented in Fig. S2 in SI). Hence, we expect the experimentally-observed $\sim$cm-scale pipes to scale up to 10-100 m in natural sediments, as observed in the field (Cartwright & Santamarina, 2015; Crutchley et al., 2021). The elongated bubble shape implies that bubble rise can happen at lower bubble volumes than that predicted by Eq. 11, as the drag force which resists the bubble migration is proportional to the cross-section in the direction of motion. As the confinement imposed by lithostatic stress reduces with the bubble height within the sediment, near the sediment surface the bubbles may resume their spherical shapes (Z. Sun & Santamarina, 2019).

5.3.2 Pockmark geometry

Our experimental observation of a transition from Type 2 to Type 1 PMs as seal thickness, h_c, increases, also correlates with deepening of PMs, i.e. experimental Type 2 PMs are generally shallower (smaller PM depth, D) than Type 1 PMs. This agrees with trends observed in the field, where D also increases with h_c (e.g. Fig 10 of Brothers et al., 2012) and Type 2 PMs are often observed to be shallower than Type 1 PMs (Riboulot et al., 2016). We speculate that the transition between the PM types may arise from fracture spacing: layer thickness controls fracture spacing (Wu & Pollard, 1995), and thus thin layers will break into smaller blocks delineated by more closely-spaced fractures, which in turn would favor creation of the complex, Type 2 PMs (e.g. experiment #1B in Fig.

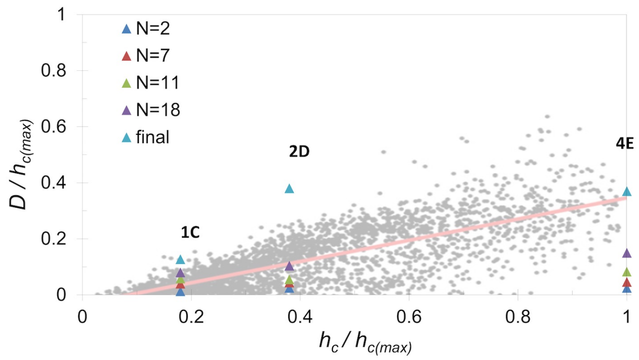

Figure 13: Comparing the pockmark depth D against clay thickness h_c between our experiments (triangles) and field observations (gray dots). To compare between the laboratory and field scale, we normalize both D and h_c by the maximal thickness $h_{c(max)}$. The value of $h_{c(max)}$ was 45 m for the field data, and 0.1 m for experiments (the value obtained in #4E). Also shown is the evolution of $D/h_{c(max)}$ with number of seepage events N (legend) for the 3 presented experiments: #1C (brittle), # 2D and # 4E (both plastic deformation); see also Fig. 7. Field data is from 3066 pockmarks offshore Maine, US (modified from Brothers et al. (2012); the pink line shows a linear trend for this population ($R^2 = 0.60$).)

6). In contrast, large fracture spacing in thick layers would favor creation of simpler Type-1 PM with seepage from only a few, widely-spaced fractures. Another feature we observed experimentally, which was also observed in the field, is that Type I PMs retain a relatively equidimensional depression shape (Fig. 5), despite the rise of elongated bubbled, as seen by Crutchley et al. (2021); Hsu et al. (2021); Marcon et al. (2021). However, in cases where doming collapse led to clay breaching, seepage from multiple points between semi-rigid clay blocks resulted in Type-2 pockmarks with uneven depression (Figs. 6, 8).

Our observation of increasing pockmark depth D with time, until it traverses the entire clay layer (i.e. approaching the clay thickness h_c) (#2D in Fig. 6), is in general agreement with field observations, e.g. Andresen et al. (2021), which relates PM deepening to gas seepage events, as a consequence of sea level drops. In addition, Brothers et al. (2012) show varying pockmark depth related to the same hosting layer thickness (their Fig. 10). A potential explanation is that the field data convolves different stages of PM development, since the depth (and thus D/h_c) changes with the number of events N (as we observed experimentally, cf. Fig. 13). We also found a progressive increase in Type 1 PM width, L, by wall collapse (Fig. 7b), in qualitative agreement with field observations of PM slopes steeper than the angle of repose, which suggest that these are active PMs, with temporarily non-stable slopes (Webb et al., 2009). The PM walls observed in our experiments are steeper than in the field (angle of $\sim 10^o$ (e.g. Rogers et al., 2006; Andrews et al., 2010; Schattner et al., 2016)). The steeper PMs in our experiments, in comparison to field observed PMs, could be due to friction reduction in the field, following multiple seepage events and material degradation at long times in nature (vs. the short time of our experiments), as well as the artifact of additional frictional resistance (between the clay and the plexiglass walls) in our quasi-2D setup.

5.4 Temporal evolution of gas escape

We observe episodic gas escape, with long quiescent periods interspersed by gas bubble ascent (either by deforming plastically the seal, or through fractures). Each seepage event is accompanied by an abrupt change in PM geometry, and weakening of the flow path (into a pipe). Similar episodic venting was seen in a north sea PM, from which gas flaring was observed in one expedition but not a few years later (Hustoft et al., 2009). Long quiescent period of over a decade with no PM geometry change was observed by (Brothers et al., 2011), implying that it would be extremely hard to observe the short episodic venting during such periods. However, since previous work suggests that stress perturbations accelerate bubble escape from sediments (Katsman, 2019), it is not surprising that most observations of episodic gas emission from PMs, follow a stress perturbations, e.g. by earthquakes and storms (Hasiotis et al., 1996; Soter, 1999; Field & Jennings, 1987; Gontz et al., 2001; Christodoulou et al., 2023). Based on our experimental observations, we hypothesize that episodicity often characterizes gas seepage from PMs: each seepage event, which also deforms the PM, reflects something akin to a magmatic eruption in a volcano: enough gas overpressure must be accumulated to overcome the overlying layer resistance to deformation and open a fracture, akin to dike opening by magma. Opening allows gas escape, which then drops the pressure until it again accumulates to cause another eruption. Finally, we note that magmatic eruptions and mud volcanoes can also occur in a continuous manner (Kelemen & Aharonov, 1998; Hidalgo et al., 2015; Fallahi et al., 2017), which, according to the above analogy, suggests a possibility of continuous gas seepage, which we did not observe in our experiments.

6 Conclusions

To understand submarine gas seeps and the associated surface deformation creating pockmarks, we developed an experimental model system composed of a reservoir (glass beads representing a sandy sediment) overlaid by a deformable seal (clay layer). We find that gas rises continuously through the reservoir and accumulates in a spatially-limited zone at the base of the seal, due to the high capillary threshold of the fine-grained clay limiting gas invasion into it. Over time, sufficient gas overpressure accumulates to deform the clay and seep through it. Gas seepage was found to occur by either (i) doming of the seal and breaching of the dome by fracturing, resulting in disordered, Type-2, pockmarks; (ii) brittle deformation that creates faults, through which the gas seeps; or (iii) plastic deformation by gas bubbles ascending through the seal; both (ii) and (iii) form Type-1 (cone shaped) pockmarks, in thicker, more compliant layers. We also observe cases where gas seeps as elongated bubbles in faults, representing mixed deformation mode. The conditions where these deformation modes govern, especially in terms of layer thickness and consolidation of the layer (determining its stiffness), were computed theoretically. We find that seepage is often assisted by a positive feedback mechanism: pipe-like preferential conduits are created by the rise of trains of bubbles, that liquefy and weaken these conduits. Faults can serve as the starting point for such pathways.

We use our table-top experiments to predict natural seepage and deformation by theoretically extrapolating our finding to field conditions. This analysis suggest that the initial stage of seal deformation by gas overpressure will create a dome (Fig. 14a, b). Seepage is expected to happen by breaching of the dome by mode I fractures leading to Type-2 pockmark in thin clay layers, and by creation of hydrofractures or by flow through existing faults that eventually form Type-1 pockmark in thicker clay layers (Fig. 14c). We hypothesize that as seen experimentally, episodic release of gas bubbles will form preferential conduits ("pipes") by locally weakening the clay in their passage, as well as progressively enlarging (in depth and width) a pockmark at the surface (Fig. 14d). Our experimental observations and theoretical analysis, which are in good agreement with field data, improves our understanding of natural pockmark formation.

Data Availability Statement

All data used to generate the figures and conclusions in the paper can be downloaded from: `https://dx.doi.org/10.6084/m9.figshare.24586926`.

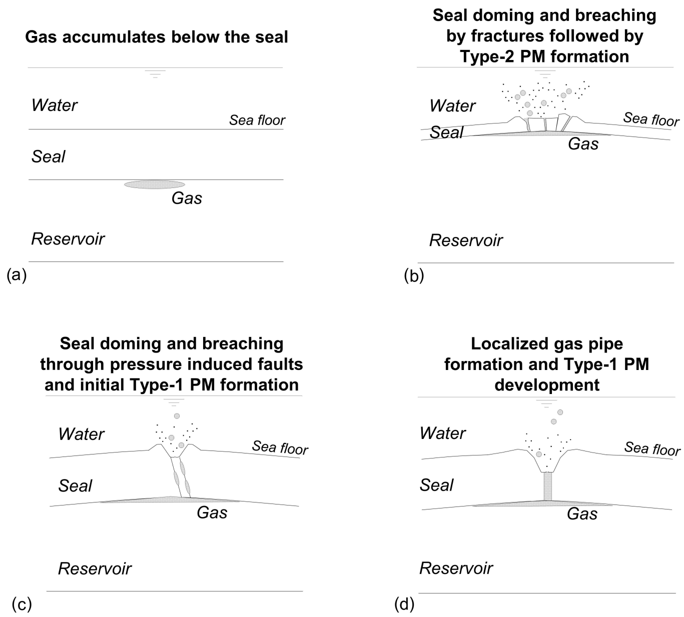

Figure 14: Schematic illustration summarizing the stages of pockmark formation expected in the field, based on theoretical insights from our experiments. (a) Gas accumulates at the top of the reservoir below the seal. Due to overpressure development the seal is deformed by doming, then gas seeps to the sea-floor thought the seal in one of the following seal breaching mechanisms: (b) Breaching of the seal by tensional fracturing. Then development of Type 2 pockmark; (c) pressure induced faults (as a consequence of brittle deformation of the seal). In this mechanism, sediment is eroded from the sea-floor and is suspended into the water by the seeping gas (sediment particles are presented as dots), progressively creating a morphological depression (Type 1 pockmark); (d) Eventually, after repeated material degradation (through the pressure induced faults presented in c), localized gas pipe through the seal is created.

Acknowledgments

RH and EH acknowledge partial support from the Ring Family Foundation for Research in Atmospheric & Global Changes Studies; RH also acknowledges partial support from the Israeli Science Foundation (#ISF-867/13), the Israel Ministry of Agriculture and Rural Development (#821-0137-13), and from the Engineering and Physical Sciences Research Council (EP/V050613/1). OK acknowledges support from the Israeli Science Foundation (#ISF-954/15).

References

Abrams, M. A. (2005). Significance of hydrocarbon seepage relative to petroleum generation and entrapment. *Marine and Petroleum Geology*, *22*(4), 457–477.

Andresen, K., Dahlin, A., Kjeldsen, K., Røy, H., Bennike, O., Nørgaard-Pedersen, N., & Seidenkrantz, M.-S. (2021). The longevity of pockmarks–a case study from a shallow water body in northern denmark. *Marine Geology*, *434*, 106440.

Andrews, B. D., Brothers, L. L., & Barnhardt, W. A. (2010). Automated feature extraction and spatial organization of seafloor pockmarks, belfast bay, maine, usa. *Geomorphology*, *124*(1-2), 55–64.

Archer, D., Buffett, B., & Brovkin, V. (2009). Ocean methane hydrates as a slow tipping point in the global carbon cycle. *Proceedings of the National Academy of Sciences*, *106*(49), 20596–20601.

Atkinson, J., Charles, J., & Mhach, H. (1994). Undrained hydraulic fracture in cavity expansion tests. In *International conference on soil mechanics and foundation engineering* (pp. 1009–1012).

Barry, M. A., Boudreau, B. P., & Johnson, B. D. (2012). Gas domes in soft cohesive sediments. *Geology*, *40*(4), 379-382. doi: 10.1130/G32686.1

Bayon, G., Loncke, L., Dupré, S., Caprais, J.-C., Ducassou, E., Duperron, S., ... others (2009). Multi-disciplinary investigation of fluid seepage on an unstable margin: the case of the central nile deep sea fan. *Marine Geology*, *261*(1-4), 92–104.

Berndt, C. (2005). Focused fluid flow in passive continental margins. *Philosophical Transactions of the Royal Society A: Mathematical, Physical and Engineering Sciences*, *363*(1837), 2855-2871. doi: 10.1098/rsta.2005.1666

Berndt, C., Bünz, S., & Mienert, J. (2003). Polygonal fault systems on the mid-norwegian margin: a long-term source for fluid flow. *Geological Society, London, Special Publications*, *216*(1), 283–290.

Bøe, R., Rise, L., & Ottesen, D. (1998). Elongate depressions on the southern slope of the norwegian trench (skagerrak): morphology and evolution. *Marine Geology*, *146*(1-4), 191–203.

Böttner, C., Berndt, C., Reinardy, B. T., Geersen, J., Karstens, J., Bull, J. M., ... Haeckel, M. (2019). Pockmarks in the witch ground basin, central north sea. *Geochemistry, Geophysics, Geosystems*, *20*(4), 1698-1719. doi: https://doi.org/10.1029/2018GC008068

Boudreau, B. P. (2012). The physics of bubbles in surficial, soft, cohesive sediments. *Marine and Petroleum Geology*, *38*(1), 1–18.

Boudreau, B. P., Algar, C., Johnson, B. D., Croudace, I., Reed, A., Furukawa, Y., ... Gardiner, B. (2005). Bubble growth and rise in soft sediments. *Geology*, *33*(6), 517–520.

Bower, A. F. (2009). *Applied mechanics of solids*. CRC press.

Brothers, L. L., Kelley, J. T., Belknap, D. F., Barnhardt, W. A., Andrews, B. D., Legere, C., & Clarke, J. E. H. (2012). Shallow stratigraphic control on pockmark distribution in north temperate estuaries. *Marine Geology*, *329*, 34–45.

Brothers, L. L., Kelley, J. T., Belknap, D. F., Barnhardt, W. A., Andrews, B. D., & Maynard, M. L. (2011). More than a century of bathymetric observations and present-day shallow sediment characterization in belfast bay, maine, usa: Implication for pockmark field longeviy. *Geo-Marine Letters*, *31*, 237–248.

Brown, K. M. (1990). The nature and hydrogeologic significance of mud diapirs and diatremes for accretionary systems. *Journal of Geophysical Research: Solid Earth*, *95*(B6), 8969–8982.

Camerlenghi, A., Cita, M., Vedova, B. D., Fusi, N., Mirabile, L., & Pellis, G. (1995). Geophysical evidence of mud diapirism on the mediterranean ridge accretionary complex. *Marine Geophysical Researches*, *17*(2), 115–141.

Cartwright, J., Huuse, M., & Aplin, A. (2007). Seal bypass systems. *AAPG bulletin*, *91*(8), 1141–1166.

Cartwright, J., & Santamarina, C. (2015). Seismic characteristics of fluid escape pipes in sedimentary basins: implications for pipe genesis. *Marine and Petroleum Geology*, *65*, 126–140.

Cathles, L. M., Su, Z., & Chen, D. (2010). The physics of gas chimney and pockmark formation, with implications for assessment of seafloor hazards and gas sequestration. *Marine and Petroleum Geology*, *27*, 82-91.

Chapuis, R. P., & Aubertin, M. (2003). On the use of the kozeny carman equation to predict the hydraulic conductivity of soils. *Canadian Geotechnical Journal*, *40*(3), 616–628.

Christodoulou, D., Papatheodorou, G., Geraga, M., Etiope, G., Giannopoulos, N., Kokkalas, S., ... others (2023). Geophysical and geochemical exploration of the pockmark field in the gulf of patras: New insights on formation, growth and activity. *Applied Sciences*, *13*(18), 10449.

Crutchley, G. J., Mountjoy, J. J., Hillman, J. I. T., Turco, F., Watson, S., Flemings, P. B., ... Bialas, J. (2021). Upward-doming zones of gas hydrate and free gas at the bases of gas chimneys, new zealand's hikurangi margin. *Journal of Geophysical Research: Solid Earth*, *126*(9), e2020JB021489. doi: https://doi.org/10.1029/2020JB021489

Davies, R. J., Mathias, S. A., Moss, J., Hustoft, S., & Newport, L. (2012). Hydraulic fractures: How far can they go? *Marine and petroleum geology*, *37*(1), 1–6.

de Mahiques, M. M., Schattner, U., Lazar, M., Sumida, P. Y. G., & de Souza, L. A. P. (2017). An extensive pockmark field on the upper atlantic margin of southeast brazil: spatial analysis and its relationship with salt diapirism. *Heliyon*, *3*(2), e00257.

Dickens, G. R. (n.d.). Rethinking the global carbon cycle with a large, dynamic and microbially mediated gas hydrate capacitor. *Earth and Planetary Science Letters*.

Dillon, W. P., Danforth, W., Hutchinson, D., Drury, R., Taylor, M., & Booth, J. (1998). Evidence for faulting related to dissociation of gas hydrate and release of methane off the southeastern united states. *Geological Society, London, Special Publications*, *137*(1), 293–302.

Dupré, S., Woodside, J., Klaucke, I., Mascle, J., & Foucher, J.-P. (2010). Widespread active seepage activity on the nile deep sea fan (offshore egypt) revealed by high-definition geophysical imagery. *Marine Geology*, *275*(1), 1–19.

Fallahi, M. J., Obermann, A., Lupi, M., Karyono, K., & Mazzini, A. (2017). The plumbing system feeding the lusi eruption revealed by ambient noise tomography. *Journal of Geophysical Research: Solid Earth*, *122*(10), 8200-8213. doi: https://doi.org/10.1002/2017JB014592

Fauria, K. E., & Rempel, A. W. (2011). Gas invasion into water-saturated, unconsolidated porous media: Implications for gas hydrate reservoirs. *Earth Planet. Sci. Lett.*, *312*(1–2), 188–193.

Field, M. E., & Jennings, A. E. (1987). Seafloor gas seeps triggered by a northern california earthquake. *Marine Geology*, *77*(1-2), 39–51.

Forwick, M., Baeten, N. J., & Vorren, T. O. (2009). Pockmarks in spitsbergen fjords. *Norwegian Journal of Geology/Norsk Geologisk Forening*, *89*.

Franchi, F., Rovere, M., Gamberi, F., Rashed, H., Vaselli, O., & Tassi, F. (2017). Authigenic minerals from the Paola Ridge (southern Tyrrhenian Sea): Evidences of episodic methane seepage. *Marine and Petroleum Geology*, *86*, 228-247. doi: https://doi.org/10.1016/j.marpetgeo.2017.05.031

García-Gil, S. (2003). A natural laboratory for shallow gas: the rías baixas (nw spain). *Geo-Marine Letters*, *23*(3), 215–229.

Gay, A., Lopez, M., Cochonat, P., Séranne, M., Levaché, D., & Sermondadaz, G. (2006). Isolated seafloor pockmarks linked to BSRs, fluid chimneys, polygonal faults and stacked Oligocene-Miocene turbiditic palaeochannels in the Lower Congo Basin. *Marine Geology*, *226*(1-2), 25–40.

Goff, J. A. (2019). Modern and fossil pockmarks in the new england mud patch: Implications for submarine groundwater discharge on the middle shelf. *Geophysical Research Letters*, *46*(21), 12213-12220. doi: https://doi.org/10.1029/2019GL084881

Gontz, A. M., Belknap, D., Daniel, F., & Kelley, J. (2001). Evidence for changes in the belfast bay pockmark field, maine. In *Geological society of america, abstracts with programs* (Vol. 33).

Harrington, P. (1985). Formation of pockmarks by pore-water escape. *Geo-Marine Letters*, *5*(3), 193–197.

Hasiotis, T., Papatheodorou, G., Kastanos, N., & Ferentinos, G. (1996). A pockmark field in the patras gulf (greece) and its activation during the 14/7/93 seismic event. *Marine Geology*, *130*(3-4), 333–344.

Hidalgo, S., Battaglia, J., Arellano, S., Steele, A., Bernard, B., Bourquin, J., … Vasconez, F. (2015). SO2 degassing at Tungurahua volcano (Ecuador) between 2007 and 2013: Transition from continuous to episodic activity. *J. Volcanol. Geotherm. Res.*, *298*, 1-14. doi: https://doi.org/10.1016/j.jvolgeores.2015.03.022

Holtzman, R., Szulczewski, M. L., & Juanes, R. (2012). Capillary fracturing in granular media. *Physical Review Letters*, *108*(26), 264504.

Hornbach, M. J., Saffer, D. M., & Holbrook, W. S. (2004). Critically pressured free-gas reservoirs below gas-hydrate provinces. *Nature*, *427*(6970), 142–4. doi: 10.1038/nature02172

Hovland, M., Gardner, J., & Judd, A. (2002). The significance of pockmarks to understanding fluid flow processes and geohazards. *Geofluids*, *2*(2), 127–136.

Hovland, M., Heggland, R., De Vries, M., & Tjelta, T. (2010). Unit-pockmarks and their potential significance for predicting fluid flow. *Marine and Petroleum Geology*, *27*(6), 1190–1199.

Hovland, M., Judd, A. G., & Burke, R. (1993). The global flux of methane from shallow submarine sediments. *Chemosphere*, *26*(1), 559–578.

Hovland, M., & Sommerville, J. H. (1985). Characteristics of two natural gas seepages in the north sea. *Marine and Petroleum Geology*, *2*(4), 319–326.

Hovland, M., Svensen, H., Forsberg, C. F., Johansen, H., Fichler, C., Fosså, J. H., … Rueslåtten, H. (2005). Complex pockmarks with carbonate-ridges off mid-norway: products of sediment degassing. *Marine geology*, *218*(1-4), 191–206.

Hsu, C.-W., Marcon, Y., Römer, M., Pape, T., Klaucke, I., Loher, M., … Bohrmann, G. (2021). Heterogeneous hydrocarbon seepage at mictlan asphalt knoll of the southern gulf of mexico. *Marine and Petroleum Geology*, 105185.

Hustoft, S., Bünz, S., Mienert, J., & Chand, S. (2009). Gas hydrate reservoir and active methane-venting province in sediments on ¡20 Ma young oceanic crust in the Fram Strait, offshore NW-Svalbard. *Earth and Planetary Science Letters*, *284*(1-2), 12–24.

Hustoft, S., Mienert, J., Bünz, S., & Nouzé, H. (2007). High-resolution 3d-seismic data indicate focussed fluid migration pathways above polygonal fault systems of the mid-norwegian margin. *Marine Geology*, *245*(1-4), 89–106.

Jain, A. K., & Juanes, R. (2009). Preferential mode of gas invasion in sediments: grain-scale mechanistic model of coupled multiphase fluid flow and sediment mechanics. *Journal of Geophysical Research: Solid Earth*, *114*, B08101.

Jedari-Eyvazi, F., Bayrakci, G., Minshull, T. A., Bull, J. M., Henstock, T. J., Macdonald, C., & Robinson, A. H. (2023). Seismic characterization of a fluid escape structure in the North Sea: the Scanner Pockmark complex area. *Geophysical Journal International*, *234*(1), 597-619. doi: 10.1093/gji/ggad078

Judd, A., & Hovland, M. (2009). *Seabed fluid flow: the impact on geology, biology and the marine environment.* Cambridge University Press.

Judd, A. G. (2003). The global importance and context of methane escape from the seabed. *Geo-Marine Letters*, *23*(3), 147–154.

Katsman, R. (2019). Methane bubble escape from gas horizon in muddy aquatic sediment under periodic wave loading. *Geophysical Research Letters*, *46*(12), 6507-6515. doi: 10.1029/2019GL083100

Kelemen, P. B., & Aharonov, E. (1998). Periodic formation of magma fractures and generation of layered gabbros in the lower crust beneath oceanic spreading ridges. *Geophysical monograph*, *106*, 267–289.

King, L. H., & MacLean, B. (1970). Pockmarks on the scotian shelf. *Geological Society of America Bulletin*, *81*(10), 3141–3148.

Koch, S., Berndt, C., Bialas, J., Haeckel, M., Crutchley, G., Papenberg, C., ... Greinert, J. (2015). Gas-controlled seafloor doming. *Geology*, *43*(7), 571–574.

Krämer, K., Holler, P., Herbst, G., Bratek, A., Ahmerkamp, S., Neumann, A., ... Winter, C. (2017). Abrupt emergence of a large pockmark field in the german bight, southeastern north sea. *Scientific Reports*, *7*(1), 1–8.

Lawal, M. A., Bialik, O. M., Lazar, M., Waldmann, N. D., Foubert, A., & Makovsky, Y. (2023). Modes of gas migration and seepage on the salt-rooted palmahim disturbance, southeastern mediterranean. *Marine and Petroleum Geology*, *153*, 106256. doi: https://doi.org/10.1016/j.marpetgeo.2023.106256

Linke, P., Pfannkuche, O., Torres, M., Collier, R., Witte, U., McManus, J., ... Nakamura, K.-i. (1999). Variability of benthic flux and discharge rates at vent sites determined by in situ instruments. *EOS transactions*, *80*(46 Fall Meet. Suppl), F509.

Loncke, L., & Mascle, J. F. S. P. (2004). Mud volcanoes, gas chimneys, pockmarks and mounds in the nile deep-sea fan (eastern mediterranean): geophysical evidences,. *Marine and Petroleum Geology*, *21*(6), 669–689.

Løseth, H., Wensaas, L., Arntsen, B., Hanken, N.-M., Basire, C., & Graue, K. (2011). 1000 m long gas blow-out pipes. *Marine and Petroleum Geology*, *28*(5), 1047–1060.

Macelloni, L., Simonetti, A., Knapp, J. H., Knapp, C. C., Lutken, C. B., & Lapham, L. L. (2012). Multiple resolution seismic imaging of a shallow hydrocarbon plumbing system, woolsey mound, northern gulf of mexico. *Marine and Petroleum Geology*, *38*(1), 128–142.

Makhnenko, R., Vilarrasa, V., Mylnikov, D., & Laloui, L. (2017). Hydromechanical aspects of co2 breakthrough into clay-rich caprock. *Energy Procedia*, *114*, 3219-3228. (13th International Conference on Greenhouse Gas Control Technologies, GHGT-13, 14-18 November 2016, Lausanne, Switzerland) doi: https://doi.org/10.1016/j.egypro.2017.03.1453

Marchi, M., Gottardi, G., & Soga, K. (2014). Fracturing pressure in clay. *Journal of Geotechnical and Geoenvironmental Engineering*, *140*(2), 04013008. doi: 10.1061/(ASCE)GT.1943-5606.0001019

Marcon, Y., Kelley, D., Thornton, B., Manalang, D., & Bohrmann, G. (2021). Variability of natural methane bubble release at southern hydrate ridge. *Geochemistry, Geophysics, Geosystems*, *22*(10), e2021GC009894. doi: https://doi.org/10.1029/2021GC009894

Mayne, P. W. (2001). Stress-strain-strength-flow parameters from enhanced in-situ tests. In *Proc. Int. Conf. on In situ measurement of soil properties and case histories, Bali* (pp. 27–47).

Mazzini, A., Ivanov, M. K., Nermoen, A., Bahr, A., Bohrmann, G., Svensen, H., & Planke, S. (2008). Complex plumbing systems in the near subsurface: Geometries of authigenic carbonates from dolgovskoy mound (black sea) constrained by analogue experiments. *Marine and Petroleum Geology*, *25*(6), 457-472. doi: https://doi.org/10.1016/j.marpetgeo.2007.10.002

McGinnis, D. F., Greinert, J., Artemov, Y., Beaubien, S. E., & Wüest, a. (2006). Fate of rising methane bubbles in stratified waters: How much methane reaches the atmosphere? *Journal of Geophysical Research: Solid Earth*, *111*(C9), 1–15. doi: 10.1029/2005JC003183

Morel-Seytoux, H. J. (1993). Capillary barrier at the interface of two layers. In D. Russo & G. Dagan (Eds.), *Water flow and solute transport in soils: Developments and applications* (pp. 136–151). Springer Berlin Heidelberg. doi: 10.1007/978-3-642-77947-3_10

Moss, J., & Cartwright, J. (2010). The spatial and temporal distribution of pipe formation, offshore namibia. *Marine and Petroleum Geology*, *27*(6), 1216–1234.

Nermoen, A., Galland, O., Jettestuen, E., Fristad, K., Podladchikov, Y., Svensen, H., & Malthe-Sørenssen, A. (2010). Experimental and analytic modeling of piercement structures. *Journal of Geophysical Research: Solid Earth*, *115*(B10). doi: https://doi.org/10.1029/2010JB007583

Neuzil, C. E. (1994). How permeable are clays and shales? *Water Resources Research*, *30*(2), 145-150. doi: https://doi.org/10.1029/93WR02930

Osborne, M. J., & Swarbrick, R. E. (1997). Mechanisms for Generating Overpressure in Sedimentary Basins: A Reevaluation1. *AAPG Bulletin*, *81*(6), 1023-1041. doi: 10.1306/522B49C9-1727-11D7-8645000102C1865D

Perrin, H., Clavaud, C., Wyart, M., Metzger, B., & Forterre, Y. (2019, Aug). Interparticle friction leads to nonmonotonic flow curves and hysteresis in viscous suspensions. *Physical Review X*, *9*, 031027. doi: 10.1103/PhysRevX.9.031027

Pilcher, R., & Argent, J. (2007). Mega-pockmarks and linear pockmark trains on the west african continental margin. *Marine Geology*, *244*(1), 15–32.

Plaza-Faverola, A., Bünz, S., & Mienert, J. (2011). Repeated fluid expulsion through sub-seabed chimneys offshore norway in response to glacial cycles. *Earth and Planetary Science Letters*, *305*(3-4), 297–308.

Plaza-Faverola, A., Westbrook, G. K., Ker, S., Exley, R. J., Gailler, A., Minshull, T. A., & Broto, K. (2010). Evidence from three-dimensional seismic tomography for a substantial accumulation of gas hydrate in a fluid-escape chimney in the nyegga pockmark field, offshore norway. *Journal of Geophysical Research: Solid Earth*, *115*(B8).

Poryles, R., Vidal, V., & Varas, G. (2016). Bubbles trapped in a fluidized bed: Trajectories and contact area. *Physical Review E*, *93*, 032904. doi: 10.1103/PhysRevE.93.032904

Ramos, G., Varas, G., Géminard, J.-C., & Vidal, V. (2015). Gas-induced fluidization of mobile liquid-saturated grains. *Physical Review E*, *92*, 062210. doi: 10.1103/PhysRevE.92.062210

Räss, L., Simon, N. S., & Podladchikov, Y. Y. (2018). Spontaneous formation of fluid escape pipes from subsurface reservoirs. *Scientific Reports*, *8*(1), 11116.

Riboulot, V., Sultan, N., Imbert, P., & Ker, S. (2016). Initiation of gas-hydrate pockmark in deep-water nigeria: Geo-mechanical analysis and modelling. *Earth and Planetary Science Letters*, *434*, 252–263.

Riedel, M., Villinger, H., Freudenthal, T., Pape, T., BÃ¼nz, S., & Bohrmann, G. (2020). Thermal characterization of pockmarks across vestnesa and svyatogor ridges, offshore svalbard. *Journal of Geophysical Research: Solid Earth*, *125*(12), e2020JB019468. doi: 10.1029/2020JB019468

Rogers, J. N., Kelley, J. T., Belknap, D. F., Gontz, A., & Barnhardt, W. A. (2006). Shallow-water pockmark formation in temperate estuaries: a consideration of origins in the western gulf of maine with special focus on belfast bay. *Marine Geology*, *225*(1-4), 45–62.

Schattner, U., Lazar, M., Harari, D., & Waldmann, N. (2012). Active gas migration systems offshore northern Israel, first evidence from seafloor and subsurface data. *Continental Shelf Research*, *48*, 167-172. doi: 10.1016/j.csr.2012.08.003

Schattner, U., Lazar, M., Souza, L., Ten Brink, U., & Mahiques, M. (2016). Pockmark asymmetry and seafloor currents in the santos basin offshore brazil. *Geo-Marine Letters*, *36*(6), 457–464.

Simonetti, A., Knapp, J. H., Sleeper, K., Lutken, C. B., Macelloni, L., & Knapp, C. C. (2013). Spatial distribution of gas hydrates from high-resolution seismic and core data, woolsey mound, northern gulf of mexico. *Marine and Petroleum Geology*, *44*, 21–33.

Skarke, A., Ruppel, C., Kodis, M., Brothers, D., & Lobecker, E. (2014). Widespread methane leakage from the sea floor on the northern us atlantic margin. *Nature Geoscience*, *7*(9), 657–661.

Soter, S. (1999). Macroscopic seismic anomalies and submarine pockmarks in the corinth–patras rift, greece. *Tectonophysics*, *308*(1-2), 275–290.

Sultan, N., Marsset, B., Ker, S., Marsset, T., Voisset, M., Vernant, a. M., . . . Drapeau, D. (2010). Hydrate dissolution as a potential mechanism for pockmark formation in the Niger delta. *Journal of Geophysical Research: Solid Earth*, *115*(B8), 1–33. doi: 10.1029/2010JB007453

Sun, Q., Wu, S., Cartwright, J., & Dong, D. (2012). Shallow gas and focused fluid flow systems in the pearl river mouth basin, northern south china sea. *Marine Geology*, *315*, 1–14.

Sun, Z., & Santamarina, J. C. (2019). Grain-displacive gas migration in fine-grained sediments. *Journal of Geophysical Research: Solid Earth*, *124*(3), 2274-2285. doi: 10.1029/2018JB016394

Svensen, H., Planke, S., Malthe-Sørenssen, A., Jamtveit, B., Myklebust, R., Eidem, T. R., & Rey, S. S. (2004). Release of methane from a volcanic basin as a mechanism for initial eocene global warming. *Nature*, *429*(6991), 542–545.

Tary, J.-B., Geli, L., Guennou, C., Henry, P., Sultan, N., Çağatay, N., & Vidal, V. (2012). Microevents produced by gas migration and expulsion at the seabed: a study based on sea bottom recordings from the sea of marmara. *Geophysical Journal International*, *190*(2), 993–1007. doi: 10.1111/j.1365-246X.2012.05533.x

Turcotte, D., & Schubert, G. (2014). *Geodynamics* (3rd ed.). Cambridge University Press. doi: 10.1017/CBO9780511843877

Ugural, A. (1999). *Stresses in plates and shells.* WCB/McGraw Hill.

Varas, G., Vidal, V., & Géminard, J.-C. (2009). Dynamics of crater formations in immersed granular materials. *Physical Review E*, *79*(2), 1–7.

Varas, G., Vidal, V., & Géminard, J.-C. (2011). Venting dynamics of an immersed granular layer. *Physical Review E*, *83*(1), 1–6.

Volfson, D., Tsimring, L. S., & Aranson, I. S. (2003, Aug). Partially fluidized shear granular flows: Continuum theory and molecular dynamics simulations. *Physical Review E*, *68*, 021301. doi: 10.1103/PhysRevE.68.021301

Webb, K. E., Hemmer, O., Lepland, A., & Gray, J. S. (2009). Pockmarks in the inner oslofjord, norway. *Geo-Marine Letters*, *29*, 111–124.

Westbrook, G. K., Thatcher, K. E., Rohling, E. J., Piotrowski, A. M., Pälike, H., Osborne, A. H., . . . Aquilina, A. (2009). Escape of methane gas from the seabed along the West Spitsbergen continental margin. *Geophysical Research Letters*, *36*(15), L15608.

Wood, D. M. (1991). *Soil behaviour and critical state soil mechanics.* Cambridge University Press. doi: 10.1017/CBO9781139878272

Wu, H., & Pollard, D. D. (1995). An experimental study of the relationship between joint spacing and layer thickness. *Journal of Structural Geology*, *17*(6), 887–905.

Supporting Information for "Gas seepage and pockmark formation from subsurface reservoirs: Insights from table-top experiment"

Inbar Vaknin,[1] Einat Aharonov*,[1] Ran Holtzman*,[2] and Oded Katz[3]

[1] *Institute of Earth Sciences, The Hebrew University of Jerusalem, Jerusalem, Israel*
[2] *Coventry University, Centre for Fluid and Complex Systems, Coventry, United Kingdom*
[3] *Geological Survey of Israel, Jerusalem, Israel**

Contents of this file

1. Text S1 to S3
2. Figures S1 to S2
3. Table S1

Additional Supporting Information (Files uploaded separately)

1. Captions for Movies S1 to S5

* einatah@mail.huji.ac.il; ran.holtzman@coventry.ac.uk

Introduction

Enclosed below as Supporting Information are analysis of gas pressure variation along the first part of two selected experiments (Text S1): Experiment #2D (plastic deformation mode that results in a Type-1 PM) and #1A (doming deformation mode that results in a Type-2 PM). Text S1 also includes data (Fig. S1) of gas pressure variations measured during the experiments with comparison to observed deformation events. Text 2 provides the dependency of the bubble radius and the clay (seal) thickness from the experiments (Fig. S2), which agrees with our theoretical prediction (Eq. 11 in main text). A detailed explanation of the choice of parameter values done for the theoretical calculation along the manuscript is given in Text 3 below. Five videos of selected experiments showing all modes of deformation described in the manuscript (doming, brittle, plastic) are also enclosed (Movies S1–S5).

Text S1. Analysis of gas pressure

In general, pressure buildup and drop cycles during the PMs formation (measured at the gas inlet syringe) follow the observed gas induced sill deformation and gas seepage events, respectively. Gas seepage requires a critical pressure value to keep the seepage conduit open, causing pressure to cycle. In the following, the pattern of pressure buildup and drop during two individual experiments (#2D: plastic deformation; #1A: doming) are described in comparison to their cyclic deformation and gas seepage events.

In the plastic deformation mode (Fig. S1a), gas pressure typically builds up until it reaches the capillary threshold of the sand. At that point, gas invades the sand layer causing a sudden drop in pressure due to the gas volume expansion. Since the capillary threshold of the sand is substantially higher than the pressure required for the plastic yielding of the clay, the first peak in Fig. S1a occurs well before breaching of the clay layer. After this peak, signifying gas invasion into the reservoir, pressure starts dropping. The pressure decrease continues while the clay layer is breached (yellow diamond marked II in Fig. S1a), which also corresponds to stage II in Fig. 3 (experiment #2D), and as gas seeps and transverses the clay layer (yellow diamonds marked III – V in Fig. S1a, and stage III–V in Fig. 3). At that point ($\sim$230 seconds) the first seepage event is finished, and the gas conduit closes. With time, pressure recovers. Once the pressure exceeds the critical threshold required to reopen the pathway through the clay, another seep event occurs and the pressure drops again to its minimum value ($\sim$600 seconds in Fig. S1a). From here on, repeated minor pressure build-ups and drops are recorded as a result of seepage events through a quasi-open pathway through the clay (e.g. yellow diamond marked VI in Fig. S1a, and snapshot VI for experiment #2D in Fig. 3).

The pressure variations in the doming deformation mode (Fig. S1b) typically evolve quite differently than the one describes above for the plastic mode. Initially, like in the plastic case, pressure builds up to the sand capillary threshold, after which it starts to drop. Pressure drop continues through doming initiation (yellow diamond marked II in Fig. S1b), which also corresponds to snapshot II in Fig. 3 (Experiment #1A) and the dome final expansion where the drop ceased (Pm1 in Fig. S1b). Then, pressure starts to build up again, and when it reaches a new critical value (Pc1 in Fig. S1b) the dome inflates abruptly (apparently due to reopening of the gas pathway), causing a pressure drop (to Pm2). Further expansion of the dome following pressure buildup (stage III) causes it to crack until it is breached (stage IV). Gas escapes through the breach (stage V) causing the pressure to drop again. Gas seepage requires a critical pressure value to keep the conduit between the clay blocks open, causing pressure to cycle, i.e. to increase when the conduit collapses and to decrease when it is reopened (similar to diking systems, e.g. Kelemen and Aharonov (1998)).

We note that during the experiments the pump heats up periodically (by 0.2^oC), and high-temperature peaks are minutes apart. At the max temperature, the injection rate decreases and results in short-duration events exhibiting a lower pressurization rate (Fig. S1).

Text S2. Analyzing bubble radius as function of clay (seal) thickness

Theoretically, we predict that bubble size increases with seal thickness (Eq. 11 in main text). Fig. S2 shows measured experimental results that verifies this dependency.

Text S3. Choice of parameter values

A complete list of parameters used in this paper and the choice of values (when applicable) is provided in Table S1. Densities of clay and water are $\rho_c = 1500$ and $\rho_w = 1000$ kg/m^3. In clay, the undrained friction angle, ϕ, is 20 - 45^o, following Ouyang and Mayne (2018). We use the lower value of $\phi = 20^o$ due to the very high water content and short settling time. In nature most soils are over-consolidated to some degree (Wood, 1991), $OCR > 1$. Here, as we used clay that settled in water under its own weight (lower normal stress than in nature), we expect the clay to be under- or normally-consolidated, $OCR \leq 1$. Thus, we use values of OCR=1 and OCR=0.5 for the experiments with $t_s = 6$ and 3 weeks, respectively. We use typical value of the exponent, $\gamma = 0.8$, following Sun and Santamarina (2019). Using the above parameter values, and the range of clay layer thickness tested here, $h_c = 0.007$ - 0.1m, Eq. 9 predicts c_u ranges of 8.5 - 85 and 4.9 - 49 Pa for t_s of 6 and 3 weeks, respectively.

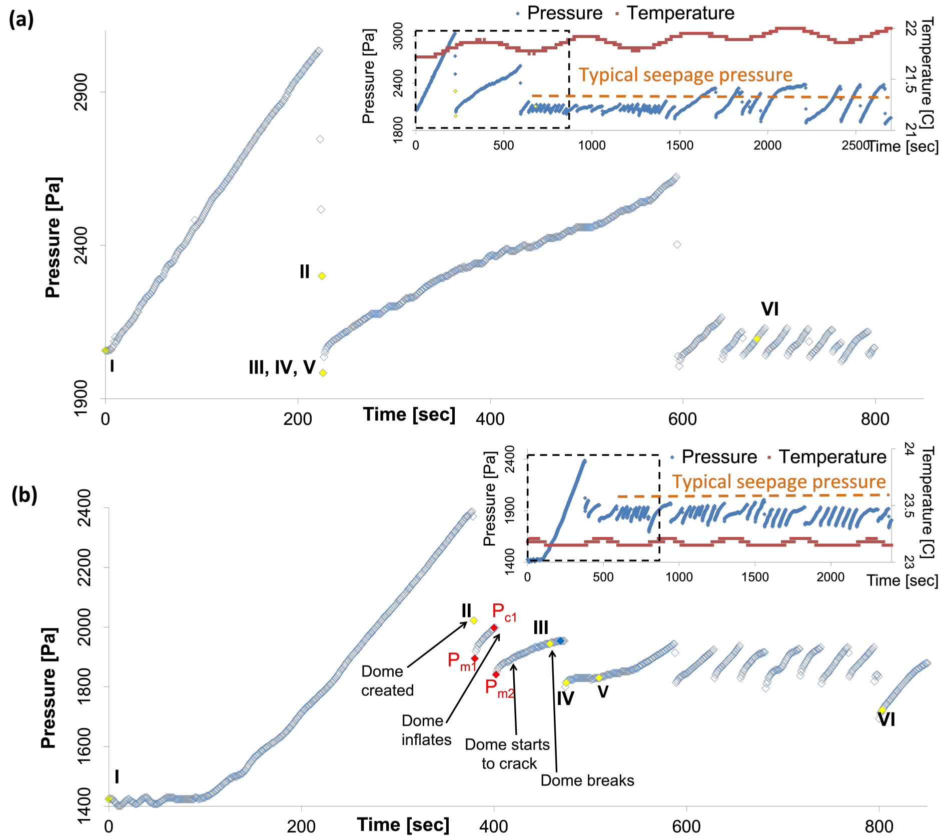

FIG. S1. Pressure variation (measured at the syringe pump outlet) along the first part of two selected experiments. (a) Experiment #2D (h_c = 3.8 cm): seal breaching by liquefaction around ascending gas bubble and development of Type-1 pockmark (see Table 1 in main text for more detail about the experimental setting). Yellow diamonds numbered I - VI are points presented by the snapshots in Fig. 3 in main text. Inset shows pressure and temperature variation along the entire experiment (dashed frame shows the time slot presented in details). Post breaching cyclic seepage pressure is marked by the orange dashed line; (b) Experiment #1A (h_c = 0.7 cm): Doming and breaching by fracturing of the dome and development of Type-2 pockmark. Yellow diamonds numbered I - VI are points presented by the snapshots in Figure 3. Inset shows pressure and temperature variation along the entire experiment (dashed frame shows the time slot presented in details). Post breaching cyclic seepage pressure is marked by the orange dashed line.

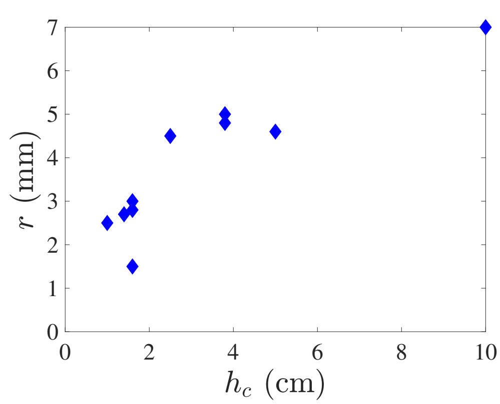

FIG. S2. Bubble radius r as a function of clay (seal) thickness h_c in experiments where the clay deformed plastically.

TABLE S1. Parameters used in the experiments and the analyses. See Text 3 for details of selection of values.

Symbol	Name	Values	Units
N	number of seepage events	0–25	-
h_c	clay layer thickness	0.007–1000	m
t_s	duration of clay settlement	3 or 6	weeks
D	pockmark depth	NA†	-
L	pockmark width	NA†	-
P_g	Gas pressure	NA†	-
P_w	Water pressure	NA†	-
ΔP	Gas overpressure	NA†	-
h_g	Gas pocket height	NA†	-
ρ_w	Water density	1000	kg/m^3
ρ_g	Gas density	1	kg/m^3
ρ_g	Clay density	1500 (experiments) 1890 (field)	kg/m^3
g	Gravitational acceleration	9.81	m/s^2
σ'_v	Effective stress (bottom of clay layer)	NA†	-
$\Delta P_{\mathrm{cavity}}$	Critical pressure to form a cavity	NA†	-
σ'_3	Effective stress (minor principal direction)	NA†	-
E	Young's modulus (of clay)	Eq. S1	Pa
ν	Poisson ratio (of clay)	0.3 [a]	-
c_u	Undrained shear strength (of clay)	Eq. 5 (main text)	Pa
ϕ	Undrained friction angle (of clay)	20	degrees
OCR	Overconsolidation ratio	0.5–1	-
r	Gas bubble radius	NA†	-
γ	Exponent relating strength and OCR	0.8 [b]	-
F_d	Drag force	NA†	-
F_b	buoyancy force	NA†	-
k	Empirical coefficient (for critical bubble radius)	NA†	-
ΔP_{dome}	Fracturing pressure (for dome)	NA†	-
ΔP_{plug}	Critical faulting pressure (for forming a plug)	NA†	-
T_0	Tensional strength (of clay)	5000-6000	Pa
a	Dome length	NA	
W	experimental cell width	15 or 50	cm
l	Plug length	1	cm
d	Spacing between cell walls (=plug thickness)	0.3	cm
F_{frac}	Faulting force	NA†	-
F_{slid}	Sliding force	NA†	-
n	Empirical factor (shear contribution to fracturing)	$\sim$1.25 [c]	-
ϕ_w	Clay-wall friction angle	7	-

† Non-applicable (e.g. parameter value continuously changes).
[a] Marchi *et al.* (2014).
[b] Sun and Santamarina (2019).
[c] Atkinson *et al.* (1994).

In computing the sliding force (Eq. 4 in main text) we use the following parameter values: $n = 1.25$ (Atkinson 2017) $\mu_c = \tan(\phi)$ and plug width of $l \approx 1$ cm (from analysis of our experimental images). For lack of measured values of the friction coefficient of udrained Kaolinite against Plexiglas, we consider a value of $\phi_w = 7^o$ (Xu *et al.* 2018).

The spacing between the plexigalss walls is $d = 3$ mm. We use $\nu = 0.3$ for the Poisson ratio of clay (Marchi *et al.* 2014). We note that the Young's modulus E increases with settlement time, t_s, due to chemo-mechanical consolidation and time-dependent changes in clay outer layer electric charge effecting bonding (Marcuson and Wahls 1972, Mukabi and Hossain 2011). To examine this effect of varying E, we used two settling times t_s, 3 and 6 weeks. Multiple studies have found that E also grows monotonically with effective stress (Ishihara 1996, Chapman and Godin 2001, Snieder and Beukel 2004). As we did not measure experimentally E, we adopt the following functional dependence of E as a function of the OCR and the effective stress (Athanasopoulos 1993):

$$E = A{\sigma'_v}^{0.58} OCR^{0.42} \tag{S1}$$

where A=20000 for the experiments and 2000 for the field. This provides E values ranging between $130kPa$ to $27MPa$ for h_c ranging from 0.01-1000 m. This approximately agrees with the range provided by (Koch *et al.* 2015).

For the field calculations we use a higher clay density of $1890kg/m^3$. For dome dimensions we use $a = 5h_c$, $w_{max} = 0.03a$ (Koch *et al.* 2015), noting the uncertainty due to the large variability in these values.

Movie captions

Movie S1. Video of experiment #1A showing doming initial deformation mode and consequent Type-2 pockmark formation as seepage continues. Lower dark layer is the sand reservoir, middle gray layer is the clay seal ($h_c = 0.7$ cm), upper dark layer is the water. For more details of the experimental conditions see Table 1 in main text.

Movie S2. Video of experiment #5E (wide experimental box) showing doming initial deformation mode and consequent Type-2 pockmark formation as seepage continues. The final pockmark is a result of integration of two seepage sites. Lower dark layer is the sand reservoir, middle gray layer is the clay seal ($h_c = 1.7$ cm), upper dark layer is the water. For more details of the experimental conditions see Table 1 in main text.

Movie S3. Video of experiment #5D showing brittle (faults bounded plug) initial deformation mode and consequent Type-1 pockmark formation as seepage continues. The final pockmark is asymmetric a result of integration of two seepage sites. Lower dark layer is the sand reservoir, middle gray layer is the clay seal ($h_c = 2.2$ cm), upper dark layer is the water. For more details of the experimental conditions see Table 1 in main text.

Movie S4. Video of experiment #2D showing plastic (bubble ascending) initial deformation mode and consequent Type-1 pockmark formation as seepage continues through damage chimney. Lower dark layer is the sand reservoir, middle gray layer is the clay seal ($h_c = 3.8$ cm), upper dark layer is the water. For more details of the experimental conditions see Table 1 in main text.

Movie S5. Video of experiment #4E (wide experimental box) showing plastic (bubble ascending) initial deformation mode and consequent Type-1 pockmark formation as seepage continues through damage chimney. Lower dark layer is the sand reservoir, middle gray layer is the clay seal ($h_c = 10.0$ cm), upper dark layer is the water. For more details of the experimental conditions see Table 1 in main text.

SUPPLEMENTARY REFERENCES

P. B. Kelemen and E. Aharonov, Periodic formation of magma fractures and generation of layered gabbros in the lower crust beneath oceanic spreading ridges, Geophysical monograph **106**, 267 (1998).

Z. Ouyang and P. W. Mayne, Effective friction angle of clays and silts from piezocone penetration tests, Canadian Geotechnical Journal **55**, 1230 (2018).

Z. Sun and J. C. Santamarina, Grain-displacive gas migration in fine-grained sediments, Journal of Geophysical Research: Solid Earth **124**, 2274 (2019).

J. Atkinson, *The mechanics of soils and foundations* (CRC press, 2017).

C. Xu, X. Wang, X. Lu, F. Dai, and S. Jiao, Experimental study of residual strength and the index of shear strength characteristics of clay soil, Engineering Geology **233**, 183 (2018).

M. Marchi, G. Gottardi, and K. Soga, Fracturing pressure in clay, Journal of Geotechnical and Geoenvironmental Engineering **140**, 04013008 (2014).

W. F. Marcuson and H. E. Wahls, Time effects on dynamic shear modulus of clays, Journal of the Soil Mechanics and Foundations Division **98**, 1359 (1972).

J. N. Mukabi and Z. Hossain, Characterization and modeling of various aspects of pre-failure deformation of clayey geomaterials–applications in modelling, in *Proceedings. 1st International Conference. on Geotechnique, Environment & construction Materials, GEOMAT, Mie, Japan* (2011).

K. Ishihara, *Soil behaviour in earthquake geotechnics* (Clarendon press Oxford, 1996).

D. M. Chapman and O. A. Godin, Dispersion of interface waves in sediments with power-law shear speed profiles. ii. experimental observations and seismo-acoustic inversions, The Journal of the Acoustical Society of America **110**, 1908 (2001).

R. Snieder and A. v. d. Beukel, The liquefaction cycle and the role of drainage in liquefaction, Granular Matter **6**, 1 (2004).

G. A. Athanasopoulos, Effects of ageing and overconsolidation on the elastic stiffness of a remoulded clay, Geotechnical & Geological Engineering **11**, 51 (1993).

S. Koch, C. Berndt, J. Bialas, M. Haeckel, G. Crutchley, C. Papenberg, D. Klaeschen, and J. Greinert, Gas-controlled seafloor doming, Geology **43**, 571 (2015).

J. Atkinson, J. Charles, and H. Mhach, Undrained hydraulic fracture in cavity expansion tests, in *International conference on soil mechanics and foundation engineering* (1994) pp. 1009–1012.